



**HAL**  
open science

## Seismology of rapidly rotating and solar-like stars

Daniel R. Reese

► **To cite this version:**

Daniel R. Reese. Seismology of rapidly rotating and solar-like stars. Solar and Stellar Astrophysics [astro-ph.SR]. Observatoire de Paris, 2018. tel-01810853

**HAL Id: tel-01810853**

**<https://theses.hal.science/tel-01810853>**

Submitted on 8 Jun 2018

**HAL** is a multi-disciplinary open access archive for the deposit and dissemination of scientific research documents, whether they are published or not. The documents may come from teaching and research institutions in France or abroad, or from public or private research centers.

L'archive ouverte pluridisciplinaire **HAL**, est destinée au dépôt et à la diffusion de documents scientifiques de niveau recherche, publiés ou non, émanant des établissements d'enseignement et de recherche français ou étrangers, des laboratoires publics ou privés.

# Habilitation for directing research

Delivered by : the Observatoire de Paris

Defended by : Daniel Roy REESE

On : May 18<sup>th</sup>, 2018

## Seismology of rapidly rotating and solar-like stars

JURY

Dr. P. KERVELLA ..... President  
Prof. J. CHRISTENSEN-DALSGAARD ..... Examiner  
Prof. M.-A. DUPRET ..... Examiner  
Dr. M.-J. GOUPIL ..... Examiner  
Dr. F. LIGNIÈRES ..... Examiner  
Prof. G. MEYNET ..... Rapporteur  
Dr. M. TAKATA ..... Rapporteur  
Prof. M. J. THOMPSON ..... Rapporteur

Laboratoire d'Études Spatiales et d'Instrumentation en Astrophysique

UMR CNRS 8109

Observatoire de Paris, Section de Meudon

5, place Jules Janssen

92195 Meudon, FRANCE





# Summary

A great deal of progress has been made in stellar physics thanks to asteroseismology, the study of pulsating stars. Indeed, asteroseismology is currently the only way to probe the internal structure of stars. The work presented here focuses on some of the theoretical aspects of this domain and addresses two broad categories of stars, namely solar-like pulsators (including red giants), and rapidly rotating pulsating stars.

The work on solar-like pulsators focuses on setting up methods for efficiently characterising a large number of stars, in preparation for space missions like TESS and PLATO 2.0. In particular, the AIMS code applies an MCMC algorithm to find stellar properties and a sample of stellar models which fit a set of seismic and classic observational constraints. In order to reduce computation time, this code interpolates within a precalculated grid of models, using a Delaunay tessellation which allows a greater flexibility on the construction of the grid. Using interpolated models based on the outputs from this code or models from other forward modelling codes, it is possible to obtain refined estimates of various stellar properties such as the mean density thanks to inversion methods put together by me and G. Buldgen, my former PhD student. Finally, I show how inversion-type methods can also be used to test more qualitative information such as whether a decreasing rotation profile is compatible with a set of observed rotational splittings and a given reference model.

In contrast to solar-like pulsators, the pulsation modes of rapidly rotating stars remain much more difficult to interpret due to the complexity of the numerical calculations needed to calculate such modes, the lack of simple frequency patterns, and the fact that it is difficult to predict mode amplitudes. The work described here therefore focuses on addressing the above difficulties one at a time in the hopes that it will one day be possible to carry out detailed asteroseismology in these stars. First of all, the non-adiabatic pulsation equations and their numerical implementation are described. The variational principle and work integrals are addressed. This is followed by a brief classification of the pulsation modes one can expect in rapidly rotating stars. I then address the frequencies patterns resulting from acoustic island modes and the interpretations of observed pulsation spectra based on these. This is then followed by a description of mode identification techniques and the ongoing efforts to adapt them to rapid rotation. Finally, the last part briefly deals with mode excitation.

# Résumé

Beaucoup de progrès ont été effectués dans la physique stellaire grâce à l’astérosismologie, l’étude des oscillations stellaires. En effet, l’astérosismologie est à l’heure actuelle la seule façon dont on dispose pour sonder la structure interne des étoiles. Le travail présenté ici concerne quelques uns des aspects théoriques de ce domaine et porte sur deux grandes catégories d’étoiles, à savoir les pulsateurs de type solaire ( $\gamma$  compris les géantes rouges), et les pulsateurs en rotation rapide.

Le travail sur les pulsateurs de type solaire se focalise sur la mise en place de méthodes capables de caractériser efficacement un grand nombre d’étoiles, ceci en anticipation de missions spatiales telles que TESS et PLATO 2.0. En particuliers, le code AIMS applique un algorithme MCMC afin de trouver les propriétés stellaires et un échantillon de modèles qui reproduisent un jeu de contraintes observationnelles sismiques et classiques. Afin de réduire le temps de calcul, ce code interpole au sein d’une grille de modèles précalculés, en s’appuyant sur une triangulation de Delaunay, ce qui permet une plus grande souplesse dans la construction de la grille. En s’appuyant sur des modèles interpolés à partir de résultats d’AIMS ou de modèles issus d’autres codes d’optimisation, il est possible d’affiner certaines propriétés stellaires, telles que la densité moyenne, grâce à des méthodes inverses mis au point par moi et G. Buldgen, mon ancien doctorant. Enfin, je montre comment des méthodes liées aux inversions permettent de tester des informations plus qualitatives telles que la possibilité ou non d’avoir un profil de rotation décroissant pour un jeu de “splittings” rotationnels<sup>1</sup> et un modèle de référence donné.

Contrairement aux pulsations de type solaire, les pulsations d’étoiles en rotation rapide demeurent beaucoup plus difficiles à interpréter à cause de la complexité des calculs numériques pour calculer de telles oscillations, l’absence de motifs simples dans les spectres de fréquences, et les difficultés qu’on a à prévoir l’amplitude de ces modes. Le travail décrit ici cherche donc à s’adresser à ces difficultés une à la fois dans l’espoir de pouvoir un jour effectuer des études astérosismiques détaillées de ces étoiles. Tout d’abord, les équations d’oscillation non-adiabatiques sont décrites ainsi que leur implémentation numérique. Le principe variationnel et l’intégrale de travail sont abordés. Ceci est suivi d’une classification succincte des modes auxquels on peut s’attendre dans une étoile en rotation rapide. J’aborde ensuite les régularités présentes dans les spectres d’oscillations de modes acoustiques d’îlots et comment celles-ci sont exploitées dans l’interprétation de spectres observés. Ceci est suivi d’une description des techniques d’identification de modes et des efforts afin de les adapter aux rotateurs rapides. Enfin, la dernière partie aborde brièvement l’excitation des modes.

---

<sup>1</sup>Espacements en fréquences provoqués par la rotation stellaire.

# Contents

<b>Summary</b>	<b>3</b>
<b>Résumé</b>	<b>4</b>
<b>1 Introduction</b>	<b>7</b>
<b>2 Solar-like pulsators</b>	<b>9</b>
2.1 Context . . . . .	9
2.2 Forward modelling with AIMS . . . . .	10
2.2.1 A brief survey of forward modelling methods . . . . .	10
2.2.2 A description of AIMS . . . . .	11
2.3 Inversions of the mean density . . . . .	12
2.4 Inequalities on rotational splittings . . . . .	17
<b>3 Oscillations of rapidly rotating stars</b>	<b>19</b>
3.1 Context . . . . .	19
3.2 Pulsation calculations . . . . .	20
3.2.1 Pulsation equations . . . . .	20
3.2.2 Numerical implementation . . . . .	23
3.2.3 Variational principle and work integral . . . . .	25
3.3 Mode classification . . . . .	27
3.3.1 Acoustic modes . . . . .	27
3.3.2 Gravito-inertial modes . . . . .	28
3.4 Frequency patterns . . . . .	29
3.4.1 An asymptotic formula for island modes . . . . .	30
3.4.2 Interpreting observations . . . . .	32
3.5 Mode identification techniques . . . . .	33
3.5.1 Multicolour mode visibilities . . . . .	34
3.5.2 Line profile variations . . . . .	36
3.6 Mode excitation . . . . .	39
<b>4 Conclusion and perspectives</b>	<b>41</b>
<b>5 Bibliography</b>	<b>45</b>

<b>A</b>	<b>Complementary note</b>	<b>51</b>
A.1	Work for the HELAS network . . . . .	51
A.2	Work for the SpaceInn network . . . . .	52
A.3	CNAP duties ( <i>i.e.</i> “tâche de service”) . . . . .	54
A.4	Teaching . . . . .	57
A.5	Supervision . . . . .	57
	A.5.1 Supervision of Master’s students . . . . .	57
	A.5.2 Supervision of PhD students . . . . .	58
<b>B</b>	<b>Curriculum Vitae</b>	<b>61</b>

# Chapter 1

## Introduction

During the past century, stellar physics has undergone much development. Indeed, progress in microphysics, fluid dynamics and numerical simulations has enabled us to gain a better comprehension of the internal structure and evolution of stars thus leading to a basic understanding of the main stages in the life of a star. At the same time, observations are helping to characterise stars in increasing detail, thereby placing tighter constraints on current stellar models and revealing their shortcomings. New instruments have enabled substantial progress in the following domains:

- **interferometry**: the combined use of multiple telescopes has led to detailed images of the shapes of nearby stars. This has revealed, in particular, the sometimes extreme centrifugal distortion of rapidly stars such as Achernar (Domiciano de Souza et al. 2003, Kervella 2016), Altair (Monnier et al. 2007), Vega (Peterson et al. 2006), and Rasalhague (Zhao et al. 2009), and has provided constraints on stellar radii and limb darkening.
- **spectropolarimetry**: the instruments ESPaDOnS (Donati 2003), Narval (Aurière 2003), HARPSpol (Piskunov et al. 2011), NeoNarval, SPIRou (Donati et al. in Deeg & Belmonte 2018), and SPIP have and will provide high-resolution polarimetric spectra of stars thereby enabling a detailed reconstruction of the magnetic fields at the stellar surface via the Zeeman Doppler Imaging technique (Semel 1989, Donati et al. 2006).
- **astrometry**: the space mission Gaia (Perryman et al. 2001) is in the process of revolutionising the field of astrometry by providing highly accurate stellar parallaxes for an unprecedented number of stars. This leads to accurate distances which in turn place tighter constraints on other stellar parameters.
- **asteroseismology**: dedicated space missions MOST (Walker et al. 2003, Matthews et al. 2004), CoRoT (Baglin et al. 2009, Auvergne et al. 2009), Kepler (Borucki et al. 2009), and BRITE (Kuschnig et al. 2009) have dramatically increased the accuracy with which stellar pulsations are observed for an ever increasing number of stars. Forthcoming missions TESS (Ricker et al. 2015) and PLATO 2.0 (Catala et al. 2011, Rauer et al. 2014) will further increase this number by covering a substantial part of the sky. In parallel, ground based instruments, such as the SONG network (Grundahl et al. 2008), are also providing spectroscopic observations of stellar pulsations which complement space-based observations.



As is the case in many scientific domains, the interpretation of these new data has revealed the limitations in our current models and how theory is lagging behind. For instance, interferometric observations have shown the importance of going beyond a 1D spherically symmetric modelling of rapidly rotating stars (*e.g.* Domiciano de Souza et al. 2003), and asteroseismic studies of red giants have shown the need for supplementary transport mechanisms in order to explain the mismatch between their internal rotation profiles and theoretical predictions (*e.g.* Eggenberger et al. 2012, Marques et al. 2013, Ceillier et al. 2013). This highlights the importance of such observations as well as the need to develop theory in order to interpret these.

The work presented here focuses on asteroseismology with an emphasis on theoretical aspects. Asteroseismology, the study of stellar pulsations, is one of the most powerful techniques for constraining stellar evolution models as it is currently the only way to probe the internal structure of stars (apart from solar neutrino detections). It has and will continue to provide a great deal of insight into stellar physics across the HR diagram as will be made clear in the present document. My research has focused on two broad categories of stars, listed here in order of increasing complexity:

1. **solar-like pulsators:** these include low-mass main-sequence stars and red giants, characterised by a large convective envelope and stochastically excited pulsation modes. The modes present in these stars tend to be acoustic modes or mixed modes (*i.e.* which behave as acoustic modes in the envelope and gravity modes in the core).
2. **rapidly rotating pulsators:** these typically correspond to intermediate mass and massive main sequence stars, which hardly have any surface convection but possess a convective core. Their pulsation modes are typically excited by the classical  $\kappa$  mechanism and can be acoustic, gravity or mixed modes.

Chapter 2 will deal with solar-like pulsators whereas Chapter 3 will address rapidly rotating pulsating stars. This will then be followed by a brief conclusion and some perspectives.

# Chapter 2

## Solar-like pulsators

### 2.1 Context

Solar-like pulsators correspond to stars with an effective temperature around 4500 to 6500 K and which harbour a convective envelope. This includes both main sequence stars in a mass range of roughly 0.8 to 1.5  $M_{\odot}$  as well as red-giants. The convection zone stochastically excites stable acoustic oscillation modes as well as mixed modes in the case of red giants. The corresponding frequency spectra contain patterns which are easy to recognise, thus allowing a clear identification of the modes in many cases, *i.e.* finding the correspondence between observed and theoretical pulsations. Accordingly, much progress has been made in the field of stellar physics thanks to the study of these stars and their oscillations, and thanks to the unprecedented observations from CoRoT and Kepler. For instance, it is possible to determine stellar properties such as mass, radius, and age to a much higher degree of accuracy (*e.g.* Metcalfe et al. 2010, Chaplin et al. 2014, Silva Aguirre et al. 2015, 2017), determine the core rotation rates of red giants (*e.g.* Beck et al. 2012, Deheuvels et al. 2012, 2014), distinguish between ascending red giant branch stars (which burn hydrogen in a shell around a helium core) and red clump stars (which burn helium in their core) (*e.g.* Mosser et al. 2012, Christensen-Dalsgaard 2014), etc. This in turn has an impact on other fields in astrophysics. For instance, obtaining precise stellar properties plays a key role in characterising stellar populations in the Milky Way and reconstructing its history (Miglio et al. 2013, Casagrande et al. 2014). Also, in order to characterise exoplanets and distinguish, for instance, between rocky planets and gaseous giants, one needs to know precisely the characteristics of the host star (see *e.g.* Guillot & Havel 2011, and references therein).

Future space missions such as TESS and especially PLATO 2.0 will dramatically increase the number of stars in which oscillations are observed. Solar-like stars are a prime target for PLATO 2.0. Indeed, the goal of this mission is to observe and characterise precisely nearby exoplanetary systems, and hence the host stars (Rauer et al. 2014). Accordingly, there are stringent requirements on the accuracy with which the mass, radius, and ages of these stars should be determined. Hence, the stellar physics community is working hard on developing asteroseismic methods which can both meet these requirements and handle the large number of stars. This work goes hand in hand with efforts to improve the physical ingredients which are used in stellar models.

Different methods exist for carrying out helio- and asteroseismic inferences, as ex-

pressed in the following quotation from Gough (1985):

Inversions can conveniently be divided into three categories. The simplest consists of the execution of the forward problem using solar models with a few adjustable parameters, and the calibration of those parameters by fitting theory to observation. The second is the use of analytical methods. [...] Thirdly, there are the formal inversion techniques borrowed from geophysics that have been used on real and artificial solar data.

The work presented in this chapter focuses on two of these three categories. Section 2.2 describes the AIMS code, a Bayesian code which applies forward modelling (*i.e.* repeated “execution of the forward problem”). Then, Sect. 2.3 describes an inversion technique for estimating the mean density of a star. Finally, Sect. 2.4 talks about consistency checks on rotational splittings in red giant stars, using the same basis as formal inversions.

## 2.2 Forward modelling with AIMS

### 2.2.1 A brief survey of forward modelling methods

The most basic type of forward modelling consists in simply scanning a grid of stellar models in search of a best fitting model. One may improve this approach and make it more sophisticated by applying a Bayesian analysis to the results, thus obtaining probability distributions for each of the stellar parameters. This is the approach taken by BASTA<sup>1</sup> (Serenelli et al. 2013, Silva Aguirre et al. 2015). One of the important questions when applying such an approach is the number of parameters to be used when setting up the grid, and the grid resolution for each of these parameters. Ideally, one would like a large set of parameters in order to test multiple aspects of stellar physics, and a high resolution in order to obtain precise results. However, one needs to limit the number of parameters and resolution in order to have a reasonable size for the grid.

One of the ways to try to overcome this limitation is to use interpolation within the grid thus allowing a lower resolution. This is the approach taken by AIMS<sup>2</sup> (Silva Aguirre et al. 2017, , Rendle et al., in prep.). Furthermore, the MCMC<sup>3</sup> algorithm used in AIMS requires being able to calculate a model at any point within the relevant parameter space. One of the issues with interpolation is interpolation errors. These need to be quantified and compared with typical observational error bars (see Rendle et al., in prep.).

Another approach is to bypass interpolation altogether by calculating models on-the-fly using a stellar evolution code. This is the approach taken in AMP<sup>4</sup> (Metcalf et al. 2009, 2014) and in Brassard et al. (2001), Charpinet et al. (2005) and Van Grootel et al. (2013)<sup>5</sup>, both of which use genetic algorithms. There is also the work by Bazot et al. (2012) where an MCMC algorithm is used instead. Calculating models on-the-fly will

---

<sup>1</sup>Bayesian STellar Algorithm.

<sup>2</sup>Asteroseismic Inferences on a Massive Scale – this is one of the codes I wrote, with the help of colleagues, during my postdoc in Birmingham as a deliverable for the SpaceInn network (see Sect. A.2).

<sup>3</sup>Monte Carlo Markov Chain

<sup>4</sup>Asteroseismic Modelling Portal, see <https://amp.phys.au.dk/>.

<sup>5</sup>We note that the models used in this approach are static models rather than the product of a stellar evolution code.

lead to the most accurate results. However, it also considerably increases the numerical cost, thus limiting the number of stars to which such an approach can be applied.

### 2.2.2 A description of AIMS

Figure 2.1 provides a flowchart which outlines how AIMS works, what sort of inputs it requires, and what sort of results are obtained. In the heart of the code is an MCMC algorithm implemented via the EMCEE python package<sup>6</sup> (Foreman-Mackey et al. 2013). The EMCEE algorithms requires an initial group of “walkers”, *i.e.* initial models or points in the parameter space, which will then progressively explore the parameter space through an iterative process based on the probabilities for each model. The probabilities associated with each model is deduced from Bayes’ theorem:

$$\underbrace{p(\theta|\mathcal{O})}_{\text{posterior}} \propto \underbrace{p(\mathcal{O}|\theta)}_{\text{likelihood}} \underbrace{p(\theta)}_{\text{priors}} \quad (2.1)$$

where  $\theta$  represents the stellar parameters and  $\mathcal{O}$  various seismic and classic observables. After a sufficient number of iterations, the group of walkers reaches a stationary state, representative of the probability distribution function (PDF) for the stellar parameters. This distribution of models can then be used to find optimal stellar parameters and associated error bars.

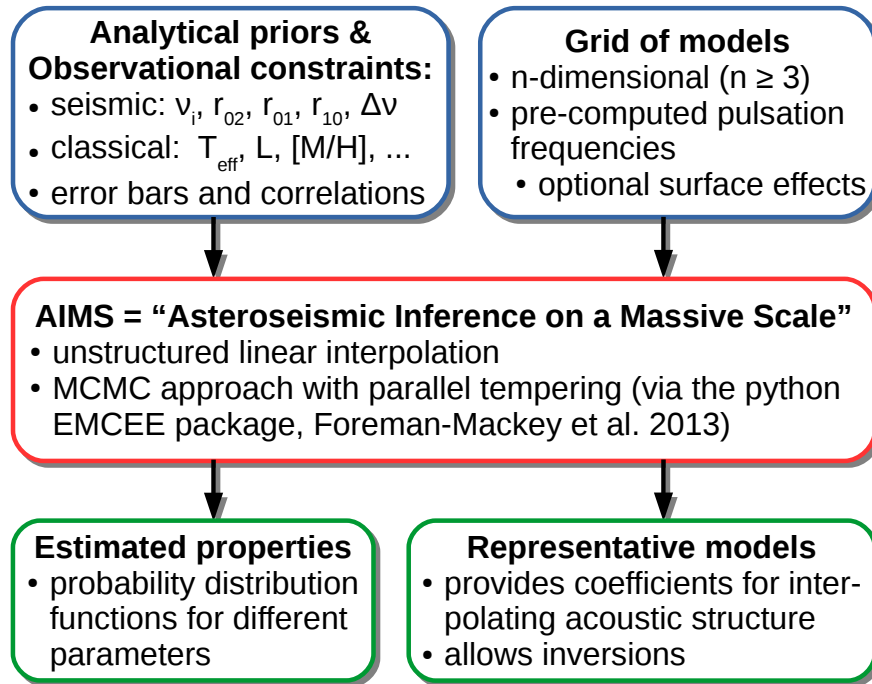


Figure 2.1: A flowchart for the AIMS code.

A second very important component of AIMS is model interpolation. This takes place in two steps:

<sup>6</sup><http://dfm.io/emcee/current/>

- **interpolation along evolutionary tracks:** this consists in carrying out a linear interpolation of the two models closest to the desired age. Rather than interpolating according to the physical age, one can choose to interpolate according to a scaled age in which each evolutionary track goes from 0 to 1. If the tracks cover comparable phases in stellar evolution (*e.g.* the main sequence), this likely leads to combining models at similar stages when interpolating between evolutionary tracks as described in the following point. A more sophisticated approach involving an equivalent age parameter is implemented in SPInS<sup>7</sup> and may be implemented in AIMS at some point in the future.
- **interpolation within the grid of models:** this is achieved thanks to a Delaunay tessellation of the parameter space excluding stellar age (see Fig. 2.2). The algorithm will search for the simplex (*i.e.* a triangle in 2D, a tetrahedron in 3D, etc.) which contains the relevant point, then perform a linear interpolation of the models at the vertices. This ensures that the interpolated quantities will remain continuous throughout the parameter space.

When interpolating between two given models, AIMS linearly combines some of the global parameters, and deduces the remaining parameters in a self-consistent way. In particular, the masses and mean densities are interpolated linearly, but the radius is deduced from the interpolated mass and mean density. The non-dimensional frequencies are interpolated linearly then rescaled using the interpolated mean density.

Figure 2.3 illustrates the sort of distribution (or sample) of models that can be obtained with AIMS for a set of observational constraints. Each subplot represents either a histogram for a given parameter or a scatter plot for two parameters, colour-coded according to the density of the points (hence, red is used for a high density of walkers and typically corresponds to models which fit the observations better). AIMS has been applied to most of the stars in the Kepler Legacy sample (Silva Aguirre et al. 2017), and has also been used to investigate the systematic effects which result from different physical ingredients or different surface correction recipes (Nsamba et al. 2018). Currently, Rendle et al. is carrying out various tests to quantify interpolation errors in AIMS, both for global quantities and mode frequencies, and to check whether the dispersion in the output set of models is truly representative of the observational error bars.

## 2.3 Inversions of the mean density

One of the drawbacks with forward modelling is its model-dependence. Hence, if a physical ingredient is missing from the models, forward modelling can at most show something is wrong with the models by producing a poor fit to the observations, but it does not provide a diagnostic as to what is wrong. To go beyond this limitation, it is necessary to be able to go outside the parameter space represented by the stellar evolution code (or the grid of models) by allowing more general modifications of the model. This is precisely what is achieved in inversion methods. Indeed, most inversion techniques rely on integral relations which relate pulsation frequency modifications to structural changes, such as the following

---

<sup>7</sup>“Stellar Parameters INferred Systematically”. This code is derived from AIMS but does not include the seismic component – see Sect. A.2.

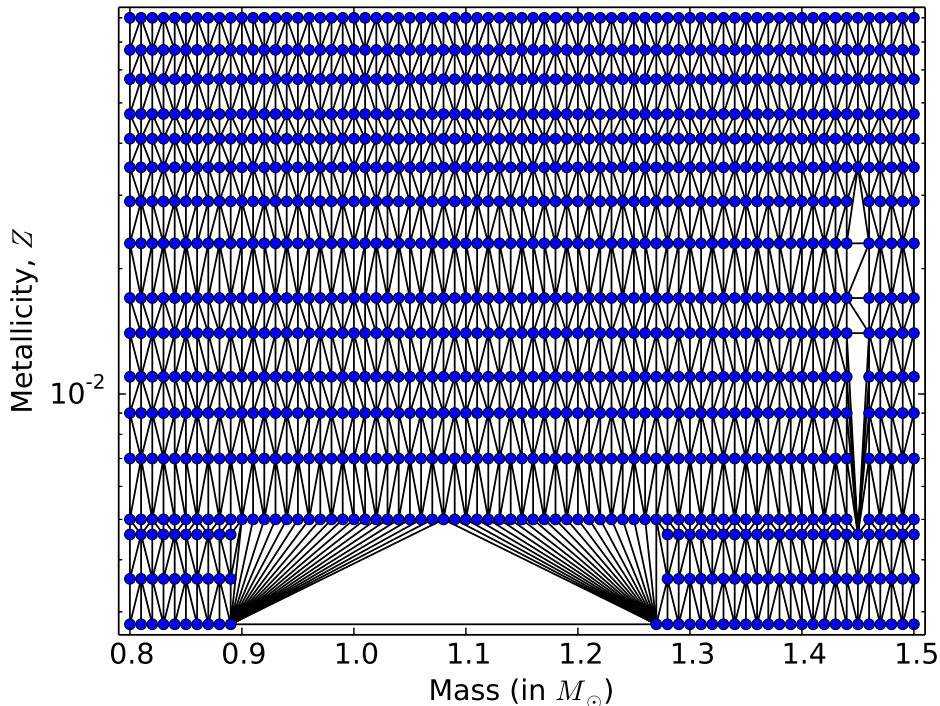


Figure 2.2: Tesselation of the grid of models by Coelho et al. (2015) and used by AIMS.

one<sup>8</sup>:

$$\frac{\delta\omega_{n,\ell}}{\omega_{n,\ell}} = \int_0^1 K_{\rho,\Gamma_1}^{n,\ell}(x) \frac{\delta\rho}{\rho} dx + \int_0^1 K_{\Gamma_1,\rho}^{n,\ell}(x) \frac{\delta\Gamma_1}{\Gamma_1} dx \quad (2.2)$$

where  $x = r/R$ ,  $\omega_{n,\ell}$  represents the frequency of a given pulsation mode,  $(n, \ell)$  its quantum numbers,  $\rho$  the density profile, and  $\Gamma_1 = (\partial \ln P / \partial \ln \rho)_{\text{ad}}$  the profile of the first adiabatic exponent. We note that a surface term has been neglected in the above expression.  $\delta$  represents a modification of the model or the difference between the observed star and the reference model used to interpret the observations – hence,  $\delta\omega_{n,\ell}$  would be derived from observations, whereas  $\delta\rho$  and  $\delta\Gamma_1$  would be unknown functions which we would like to constrain.  $K_{\rho,\Gamma_1}^{n,\ell}$  and  $K_{\Gamma_1,\rho}^{n,\ell}$  are structural kernels which quantify the pulsation mode’s response to a structural change. These kernels are obtained by perturbing an integral relation between the pulsation frequencies and their corresponding pulsation modes and making use of the variational principle (Gough & Thompson 1991, see also Sect. 3.2.3). The above kernels can then be transformed into kernels for other structural quantities using various methods (*e.g.* Buldgen et al. 2017b).

At this point, two different strategies exist for carrying out the inversion. The first consists in discretising the unknown structural profiles ( $\delta\rho$  and  $\delta\Gamma_1$  in our case) and adjusting them, typically through a regularised least-squares (RLS) fit, so as to reproduce

<sup>8</sup>We note that some inversion techniques rely on an entirely different methodology involving internal phases of the pulsation modes (*e.g.* Vorontsov et al. 2013, Roxburgh 2015) or the additive constant from Tassoul’s asymptotic formula (Roxburgh 2016).

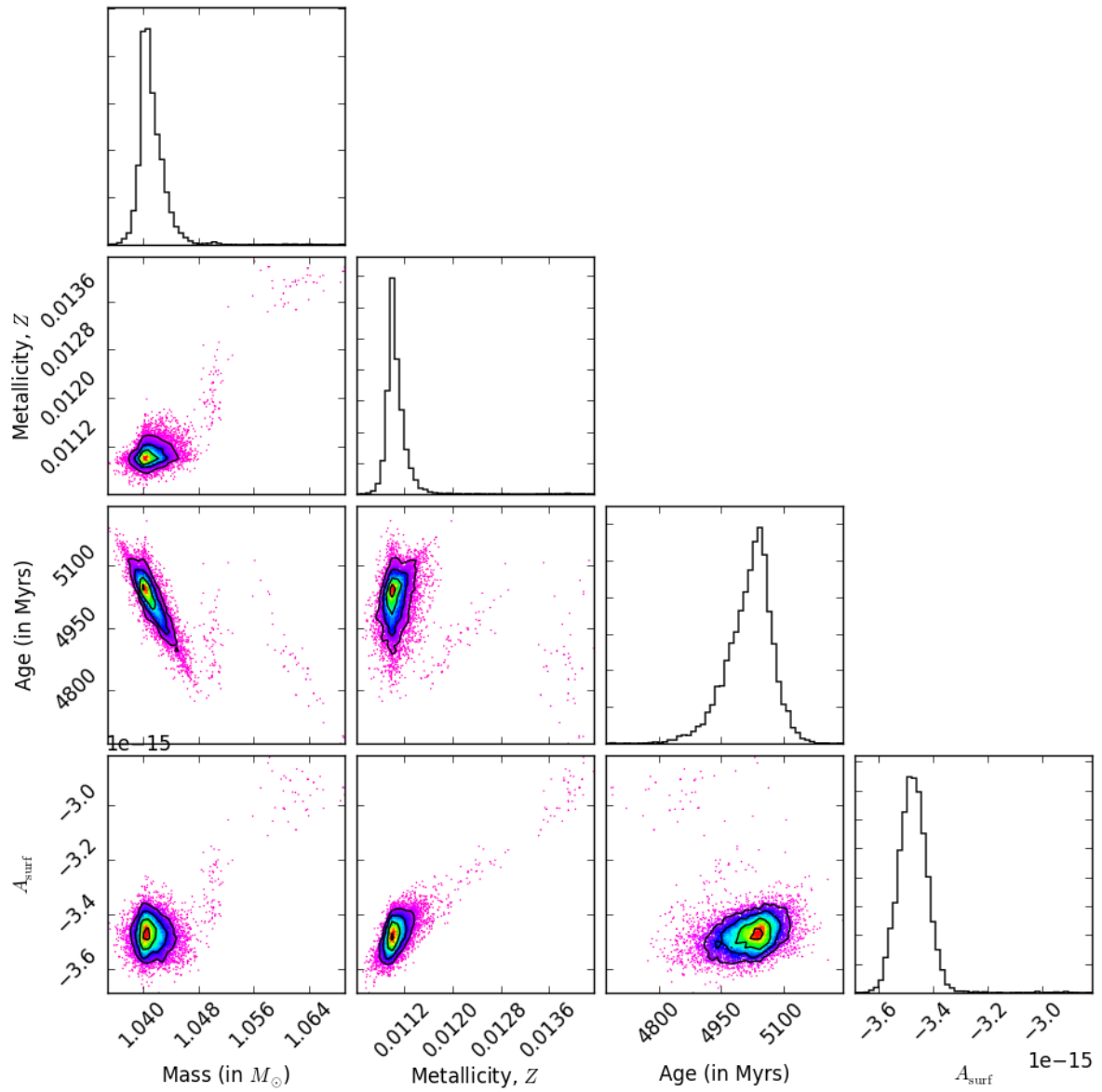


Figure 2.3: Set of plots which show the distribution of models obtained for a set of classic and seismic constraints on KIC 10963065.

the  $\delta\omega_{n,\ell}/\omega_{n,\ell}$ . In the case of a linear method, the inverted value of say the density modification,  $\delta\rho_{\text{inv}}/\rho$ , at some point  $x_0$  will be a linear combination of the frequency shifts. As pointed out in (Christensen-Dalsgaard et al. 1990), the coefficients from this linear combination,  $c_{n,\ell}$ , can then be used to construct an ‘‘averaging kernel’’,  $K_{\text{avg}}$ , and a ‘‘cross-term’’ kernel,  $K_{\text{cross}}$ :

$$\frac{\delta\rho_{\text{inv}}}{\rho}(x_0) = \sum_i c_i \frac{\delta\omega_i}{\omega_i} = \int_0^1 K_{\text{avg}}(x) \frac{\delta\rho}{\rho} dx + \int_0^1 K_{\text{cross}}(x) \frac{\delta\Gamma_1}{\Gamma_1} dx \quad (2.3)$$

$$K_{\text{avg}}(x) = \sum_i c_i K_{\rho,\Gamma_1}^i(x) \quad (2.4)$$

$$K_{\text{cross}}(x) = \sum_i c_i K_{\Gamma_1,\rho}^i(x) \quad (2.5)$$

where  $i$  is shorthand for  $(n, \ell)$  and where we made use of Eq. (2.2). The averaging and cross-term kernels therefore show the true relation between  $\delta\rho_{\text{inv}}/\rho$  and  $(\delta\rho/\rho, \delta\Gamma_1/\Gamma_1)$ . Ideally, one would like  $K_{\text{avg}}$  to be small everywhere, except at  $x_0$ , and have an integral equal to 1, in order to provide a good estimate of  $(\delta\rho_{\text{inv}}/\rho)(x_0)$ . Likewise,  $K_{\text{cross}}$  needs to be small everywhere in order to reduce the cross-talk from  $\delta\Gamma_1/\Gamma_1$ .

The second inversion strategy consists in directly optimising  $K_{\text{avg}}$  and  $K_{\text{cross}}$ . In the Subtractive Optimally Localised Averages inversion method (SOLA Pijpers & Thompson 1992, 1994), one tries to minimise the difference between  $K_{\text{avg}}$  and a target function, and likewise for  $K_{\text{cross}}$ . A narrow Gaussian function is typically used as a target function for  $K_{\text{avg}}$  as it is impossible to reproduce a perfect Dirac function.

Using the above strategies, various rotation and structural inversions have been carried out for the sun (*e.g.* Basu et al. 1997, Schou et al. 1998, Thompson et al. 2003). In the case of stars other than the sun, it is possible to carry out rotation inversions (*e.g.* Deheuvels et al. 2012, 2014) but structural inversions remain difficult given that two functions are being inverted simultaneously (as opposed to rotation inversions). However, one can still use structural inversions to constrain global stellar properties using a careful choice of the target function in a SOLA-type inversion. For instance, the following target function in a  $(\rho, \Gamma_1)$  inversion leads to an estimate of the relative difference in mean density between the observed star and the reference model, as was shown in Reese et al. (2012):

$$T(x) = 4\pi x^2 \frac{\rho(x)}{\rho_R} \quad (2.6)$$

where  $\rho_R = M/R^3$ . This inversion is linear, meaning that if the mean density of the reference model is very different from that of the observed star, the inverted mean density will be rather inaccurate. However, as was shown in Reese et al. (2012), one can carry out the inversion, rescale the reference model to the inverted mean density, and repeat the inversion and rescaling till convergence. This leads to following formula for the final mean density estimate:

$$\rho_{\text{inv}} = \rho_{\text{ref}} \left( \frac{1}{2} \sum_i c_i \frac{\omega_i^{\text{obs}}}{\omega_i^{\text{ref}}} \right)^2 \quad (2.7)$$

where  $\rho_{\text{inv}}$  is the inverted mean density,  $\rho_{\text{ref}}$  the mean density of the reference model, and  $c_i$  the inversion coefficients. This extended form is more robust to large differences be-



tween the reference and observed models. Even then, if the two have completely different structures, the results will be poor.

The left panel of Fig. 2.4 shows inversion results for  $\alpha$  Cen B using a set of 93 reference models. As can be seen, although the reference models have very different mean densities, the inverted mean densities span a much smaller range of values, thus showing the efficiency of the method. In the same plots, results from Kjeldsen et al. (2008), the  $\Delta\nu \propto \sqrt{\rho}$  scaling law, and a scaling law based on Kjeldsen et al. (2008) are shown. A comparison of these different approaches show that the SOLA inversion is comparable to the results and the scaling law from Kjeldsen et al. (2008). The  $\Delta\nu$  scaling law leads to somewhat different results with a larger dispersion, probably as a result of surface effects. The right panel shows the averaging kernel for one of the inversions. Furthermore, averaging kernels for the  $\Delta\nu$  and the Kjeldsen et al. (2008) scaling laws are shown – as was shown in Reese et al. (2012), it is possible to express these scaling laws in differential form, extract the equivalent of inversion coefficients, and produce averaging kernels from these. As can be seen, the  $\Delta\nu$  scaling law produces a highly oscillatory averaging kernel which is further from the target function than the two other averaging kernels, especially near the surface, thus explaining its high sensitivity to surface effects.

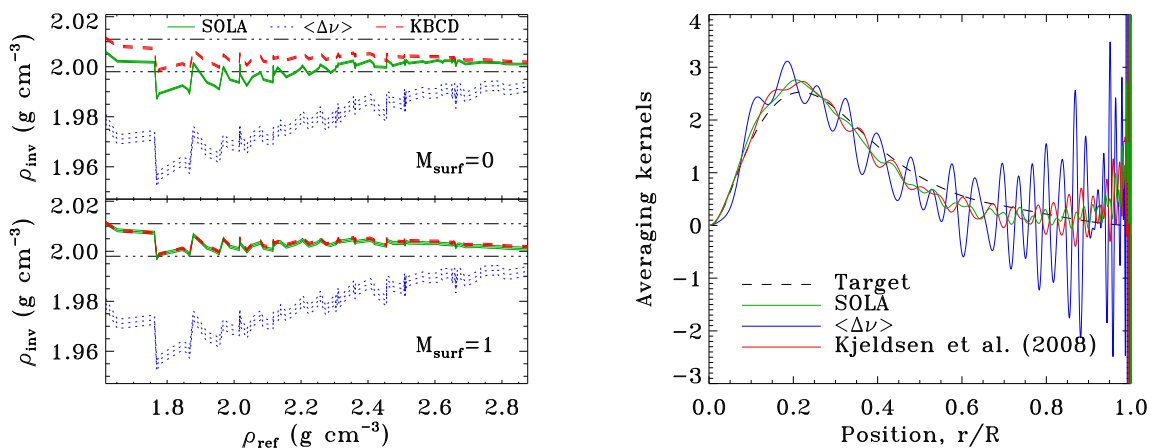


Figure 2.4: (Left) Mean density inversion results for  $\alpha$  Cen B for a set of 93 models. The x-axis indicates the mean densities of the reference models whereas the y-axis corresponds to the inverted mean densities. The horizontal dashed triple dot black lines show the mean density estimates from Kjeldsen et al. (2008). SOLA corresponds to the inversions,  $\langle \Delta\nu \rangle$  to the simple  $\Delta\nu$  scaling law, and KBCD to the scaling law deduced from Kjeldsen et al. (2008). The inversions in the upper panel have no surface correction terms, whereas the lower panel corresponds to one surface correction term in the inversions. (Right) Averaging kernels for a mean density inversion (“SOLA”), a simple  $\Delta\nu$  scaling law, and a scaling law derived from Kjeldsen et al. (2008). The target function is shown as a dashed black line (figures based on Reese et al. 2012).

As described in Sects. A.5.1 and A.5.2, G. Buldgen pursued this work by extending the method to other global quantities, namely the acoustic radius, an age indicator based on the small frequency separation, and various internal structure and mixing indicators, and by applying these inversions to various stars (Buldgen et al. 2015b,a, 2016a,b, 2017b,a,

2018). The next step is to systematically apply some of these global inversions to outputs from the AIMS code in order to refine the estimates of some of the stellar properties. This has already partially implemented thanks to the `InterpolateModel` program which produces interpolated models using the interpolation coefficients from AIMS, and the `InversionPipeline` program which systematically applies some of the above inversions (see Sect. A.2).

## 2.4 Inequalities on rotational splittings

More subtle information can be gleaned from inverse type methods. Indeed, as was shown in Reese (2015), it is possible to test whether a decreasing rotation profile or one which satisfies Rayleigh’s stability criterion<sup>9</sup> is compatible with a set of rotational splittings and a given reference model. To illustrate how this works, I first recall the relationship between a rotational splitting and the rotation profile (assuming the rotation profile only depends on  $r$ , the radial coordinate):

$$\begin{aligned} s_{n,\ell} \equiv \frac{\omega_{n,\ell,-m} - \omega_{n,\ell,0}}{m} &= (1 - C_{n,\ell}) \int_0^R K_{n,\ell}(r) \Omega(r) dr \\ &= (1 - C_{n,\ell}) \left[ \Omega(R) - \int_0^R \frac{d\Omega}{dr} I_{n,\ell}(r) dr \right] \end{aligned} \quad (2.8)$$

where  $s_{n,\ell}$  is a rotational splitting,  $\omega_{n,\ell,m}$  the pulsation frequency of the mode with quantum numbers<sup>10</sup>  $(n, \ell, m)$ ,  $C_{n,\ell}$  the Ledoux constant (Ledoux 1951),  $K_{n,\ell}(r)$  the relevant rotation kernel,  $I_{n,\ell}(r) = \int_0^r K_{n,\ell}(r') dr'$  the integrated rotation kernel, and  $\Omega(r)$  the rotation profile. The last equality was obtained by doing an integration by parts and making use of the fact that  $\int_0^R K_{n,\ell}(r) dr = 1$ . As pointed out in Reese (2015), the functions  $K_{n,\ell}(r)$  are positive (and strictly so apart from isolated points). Hence, the functions  $I_{n,\ell}(r)$  are strictly positive except for  $r = 0$ . Furthermore, they tend to line up for similar values of  $\ell$  as can be seen in the left panel of Fig. 2.5.

We then need to consider two modes, labelled  $i$  and  $j$  (which is shorthand for  $(n, \ell)$  and  $(n', \ell')$ ). If one can then find two positive constants such that:

$$aI_j(r) \leq I_i(r) \leq bI_j(r), \quad \text{for} \quad 0 \leq r \leq R \quad (2.9)$$

then multiplying this inequality by  $-\frac{d\Omega}{dr}$ , which we assume is positive, and integrating from 0 to  $R$  leads to the following inequality:

$$a [s'_j - \Omega(R)] \leq [s'_i - \Omega(R)] \leq b [s'_j - \Omega(R)], \quad (2.10)$$

where  $s'_i = s_i/(1 - C_i)$ , and where we’ve made use of Eq. (2.8). If  $\Omega(R) \geq 0$ , this inequality may be simplified to a  $s'_j \leq s'_i \leq bs'_j$  although this is a less restrictive condition. Another variant of this inequality, which is possibly more constraining, may be obtained by excluding the centre of the star and choosing an upper bound on  $-\frac{d\Omega}{dr}$  over the excluded region. Also, it is possible to combine the information from multiple modes and come up

<sup>9</sup>According to this criterion, the angular momentum must increase as the distance to the rotation axis increases, otherwise a dynamical instability will set in.

<sup>10</sup>Here, we are using the “retrograde” convention, *i.e.*, modes with positive  $m$  values are retrograde.

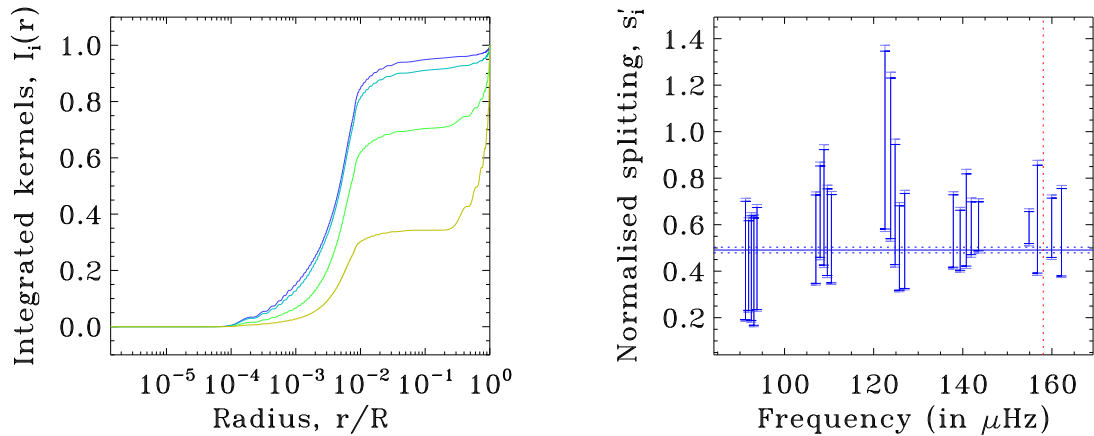


Figure 2.5: (Left) Integrated rotation kernels for several modes. (Right) A comparison between an observed rotational splitting (horizontal solid line) with its error bars (horizontal dotted lines) and inequalities based on the assumption of a decreasing rotation profile (vertical segments – the light blue extensions show the error bars). The vertical dotted line shows the frequency of the mode being tested. As can be seen, the inequalities break down just above 120  $\mu\text{Hz}$  and around 150  $\mu\text{Hz}$  (taken from Reese 2015).

with other inequalities. Finally, equivalent inequalities may be obtained for Rayleigh’s stability criterion.

If the rotational splittings fail to meet this inequality then either the assumption  $\frac{d\Omega}{dr} \leq 0$  is false, or the reference model with which the rotation kernels are calculated is a poor match to the observed star. The right panel of Fig. 2.5 shows an example where some of the inequalities break down in a red giant model. The cause for this break down is a mismatch of the density profiles between the observed target and the reference model used in the interpretation, in the upper 0.5% of the star. Because of this mismatch, the pulsation modes in the reference model have slightly different relative sensitivities to the core and the surface of the star compared to the modes in the observed target. However, such differences in sensitivity may be masked by correcting the pulsation frequencies with surface correction recipe such as the one proposed in Kjeldsen et al. (2008), thus showing the need for surface effect corrections which also correct the pulsation modes.

# Chapter 3

## Oscillations of rapidly rotating stars

### 3.1 Context

Stellar rotation is one of the major obstacles in the study of stellar evolution and the interpretation of stellar pulsations. Indeed, two new forces are introduced: the centrifugal and Coriolis forces. These cause stellar deformation, a non-uniform surface temperature known as gravity darkening, baroclinic flows which include both meridional circulation and differential rotation, various forms of turbulence, and the transport of chemical species and angular momentum (*e.g.* Maeder 2009). Nonetheless, rapidly rotating stars play an important role in several domains of astrophysics. Indeed, the majority of massive and intermediate mass stars are rotating rapidly (Royer 2009). Massive stars dominate the evolution and structure of galaxies thanks to their winds, their radiation, the resultant supernovae and the chemical enrichment of the interstellar medium (Zinnecker & Yorke 2007). Intermediate masses represent the upper limit on stars which host exoplanets (see <http://exoplanets.org>). Furthermore, many intermediate mass stars, notably  $\delta$  Scuti stars, have very rich pulsational spectra (Poretti et al. 2009). Primordial stars are very likely rapidly rotating because they are compact and they lose little mass and angular-momentum (Ekström et al. 2008). However, these are the stars which reionised the early universe and which started the production of heavier elements. Finally, rapid rotation plays a critical role in the precursors to gamma ray bursts. Indeed, all of the scenarios which are currently proposed require a very large amount of angular momentum (see Woosley & Heger 2006, and references therein).

Modelling rapidly rotating stars has already yielded a number of interesting results. As succinctly stated in Meynet & Maeder (2005a):

Rotating models can reproduce the chemical enrichments observed at the surface of OBA stars (Heger & Langer 2000, Meynet & Maeder 2000), the number ratio of blue to red supergiants in the Small Magellanic Cloud (Maeder & Meynet 2001), the variation with the metallicity of the number ratio of Wolf-Rayet to O type stars (Meynet & Maeder 2003) as well as of the type Ibc to type II supernovae (Prantzos & Boissier 2003, Meynet & Maeder 2005b).

However, various recent observations of early B-type stars in the Large Magellanic Cloud have shown mismatches between the nitrogen enrichment and theoretical expectations (Hunter et al. 2008, Brott et al. 2011). Galactic O stars, nonetheless, are in better

agreement with theoretical expectations (Martins et al. 2017). Furthermore, most of these models are based on the assumption that turbulence is much stronger in the horizontal rather than vertical direction, thereby causing a “shellular” rotation profile (*i.e.*, a profile which depends on isobars only) and an essentially 1D formalism (Zahn 1992). However, it is not clear up to what rotation rates such an approach is valid. Recently, rotation profiles have been self-consistently calculated from baroclinic effects in the 2D *Evolution STEllaire en Rotation* (ESTER) code (Rieutord & Espinosa Lara 2013, Espinosa Lara & Rieutord 2013, Rieutord et al. 2016). These depend on latitude thus departing from a shellular profile. Finally, most of these models have not been tested through asteroseismology – it is only their surface quantities which have been compared with observations.

Carrying out asteroseismology in rapidly rotating stars is by no means a straightforward task. As was highlighted in Reese et al. (2006), and as is shown by interferometric observations (*e.g.* Domiciano de Souza et al. 2003, Kervella & Domiciano de Souza 2006, Monnier et al. 2007), only a 2D approach will allow us to model rapidly rotating stars and their oscillations. Coming up with accurate 2D pulsation calculations has only been achieved in recent years with the advent of improved computing capabilities as well as highly accurate pulsation codes (*e.g.* Reese et al. 2006, Ouazzani et al. 2012). Furthermore, identifying modes, *i.e.* finding the correspondence between observed pulsations and their theoretical counterparts, is not a straightforward task (*e.g.* Goupil et al. 2005 and Fig. 5 of Deupree 2011). Nonetheless, this is a prerequisite before carrying out detailed asteroseismology. Finally, given that it is mainly massive and intermediate mass stars which rotate rapidly, the pulsation modes in such stars are excited, for the most part, by the  $\kappa$  mechanism. Such a mechanism leads to a non-linear saturation of mode amplitudes and couplings between different modes (*e.g.* Dziembowski et al. 1988). Accordingly, current theory is not able to predict the amplitudes of these modes. As a result, it has not yet been possible to carry out the same type of detailed asteroseismic deductions as what has been achieved for solar-like pulsators.

In order to address some of the above difficulties, a substantial part of my research has focused on the theoretical aspects related to pulsations in rapidly rotating stars. This work will be presented in the following sections. Section 3.2 will describe the pulsation equations in rapidly rotating stars, both in the adiabatic and non-adiabatic cases, and their implementation in a numerical code. This will be followed by a description of the variational principle as well as the work integral for non-adiabatic calculations. Section 3.4 will deal with frequency patterns obtained for a particular class of acoustic modes at rapid rotation rates, as well as observations which seem to confirm these predictions. This will be followed by a description of the observational signatures which can be used in mode identification strategies, namely amplitude ratios, phase differences, and line-profile variations (LPVs). The final section will briefly deal with mode excitation.

## 3.2 Pulsation calculations

### 3.2.1 Pulsation equations

In order to obtain the pulsation equations, one first has to start off with an equilibrium model of a rotating star.  $\Omega$  will denote its rotation profile. At this point, it is interesting to distinguish between stars with a conservative rotation profile and those with a non-

conservative profile. When the rotation profile is conservative, the centrifugal force derives from a potential, and the structure of the star is barotropic, *i.e.* lines of constant density and pressure coincide (as can be seen by taking the curl of Euler's equation). It turns out that a necessary and sufficient condition for a rotation profile to be conservative is that it only depends on the distance to the rotation axis, *i.e.* it is cylindrical. A good example of models with conservative rotation profiles are SCF models (Jackson et al. 2005, MacGregor et al. 2007). Such stellar models, however, do not respect energy conservation *locally*. Indeed, due to the propagation of energy, isotherms tend to take on a more spherical shape compared to isobars, thus leading to a baroclinic structure where isobars and isochores do not coincide. This baroclinic stellar structure in turn leads to a non-conservative differential rotation profile (see, *e.g.* Fig. 3.1) and meridional circulation. As mentioned above, Zahn (1992) proposed an approximate way of modelling such phenomena including the resultant transport of chemical elements thanks to the assumption that horizontal turbulence is much stronger than vertical turbulence, thus leading to a shellular rotation profile. This approach is essentially 1D and has accordingly been included in various stellar evolution codes (*e.g.* Palacios et al. 2003, Eggenberger et al. 2008, Marques et al. 2013). At more rapid rotation rates, a full 2D approach is necessary to model such stars. This has recently been achieved in the ESTER code in which the effects of stellar evolution are in the process of being included (Rieutord & Espinosa Lara 2013, Espinosa Lara & Rieutord 2013, Rieutord et al. 2016).

The equilibrium model is then perturbed by the pulsations. The pulsations are assumed to have a small amplitude. Thus, second order or higher order terms, resulting for instance from the product of perturbations, are neglected. This assumption considerably simplifies the system of equations by only retaining linear terms, but also makes it impossible to predict the pulsation amplitudes, when these are excited by the  $\kappa$  mechanism. The pulsations are assumed to have a time dependence of the form  $\exp(i\omega t)$ . Finally, the star is assumed to be symmetric with respect to the rotation axis. Accordingly, pulsation modes will have an azimuthal dependence of the form  $\exp(im\phi)$  where  $m$  is the azimuthal order and  $\phi$  the azimuthal angle<sup>1</sup>. This leads to the following system of equation in an inertial frame of reference:

$$0 = \frac{\delta\rho}{\rho_0} + \vec{\nabla} \cdot \vec{\xi}, \quad (3.1)$$

$$0 = [\omega + m\Omega]^2 \vec{\xi} - 2i\vec{\Omega} \times [\omega + m\Omega] \vec{\xi} - \vec{\Omega} \times (\vec{\Omega} \times \vec{\xi}) - \vec{\xi} \cdot \vec{\nabla} (s\Omega^2 \vec{e}_s) - \frac{P_0}{\rho_0} \vec{\nabla} \left( \frac{\delta P}{P_0} \right) + \frac{\vec{\nabla} P_0}{\rho_0} \left( \frac{\delta\rho}{\rho_0} - \frac{\delta P}{P_0} \right) - \vec{\nabla} \Psi' + \vec{\nabla} \left( \frac{\vec{\xi} \cdot \vec{\nabla} P_0}{\rho_0} \right) + \frac{(\vec{\xi} \cdot \vec{\nabla} P_0) \vec{\nabla} \rho_0 - (\vec{\xi} \cdot \vec{\nabla} \rho_0) \vec{\nabla} P_0}{\rho_0^2} \quad (3.2)$$

$$0 = \Delta \Psi' - 4\pi G \left( \rho_0 \frac{\delta\rho}{\rho_0} - \vec{\xi} \cdot \vec{\nabla} \rho_0 \right), \quad (3.3)$$

<sup>1</sup>The above forms for the time and azimuthal dependencies lead to what could be called the “retrograde” convention, *i.e.* modes with a positive  $m$  value correspond to retrograde modes. The opposite convention, where positive  $m$  values correspond to prograde modes, can be achieved by taking a time dependence of the form  $\exp(-i\omega t)$ .

where  $\delta$  denotes a Lagrangian perturbation, a prime ' an Eulerian perturbation, the subscript "0" equilibrium quantities,  $\vec{\xi}$  the Lagrangian displacement,  $\rho$  the density,  $P$  the pressure,  $\Psi$  the gravitational potential, and  $G$  is the gravitational constant. The first of these equations is the continuity equation and expresses the conservation of matter. The second is Euler's equation and corresponds to the conservation of momentum. The third equation is Poisson's equation and relates the gravitational potential to the distribution of matter. The above system of equation is written for the general baroclinic case. If the star were barotropic, the last term in Euler's equation would vanish. One effect which is not taken into account is meridional circulation. This is, however, expected to play a marginal role given the small velocities involved.

This system of equations needs to be completed as it contains one more unknown than equations. A simple way of closing this system is by including the adiabatic relation:

$$\frac{\delta P}{P_0} = \Gamma_1 \frac{\delta \rho}{\rho_0} \quad (3.4)$$

where  $\Gamma_1 = (\partial \ln P / \partial \ln \rho)_{\text{ad}}$  is the first adiabatic exponent. Imposing this equation amounts to neglecting heat transfers during the oscillatory motions, an approximation which is well verified in the stellar interior but not near the surface. Accordingly, the pulsation frequencies obtained this way remain very accurate, but it is not possible to calculate which modes are excited by the  $\kappa$  mechanism (or other mode excitation mechanisms excluding stochastic excitation).

In order to include heat transfers during the oscillatory motions and hence carry out a full non-adiabatic calculation, one must deal with the equation of energy conservation. The unperturbed form is:

$$T_0 \frac{dS_0}{dt} = \epsilon_0 - \frac{\vec{\nabla} \cdot \vec{F}_0}{\rho_0} \quad (3.5)$$

where  $T$  corresponds to temperature,  $S$  to entropy,  $\epsilon$  to the energy production rate (mainly from nuclear reactions), and  $\vec{F}$  to the energy flux (Dupret, PhD Thesis, page 274). Perturbing this equation with a pulsation mode yields:

$$i(\omega + m\Omega)\rho_0 T_0 \delta S = \epsilon_0 \rho_0 \left( \frac{\delta \epsilon}{\epsilon_0} + \frac{\delta \rho}{\rho_0} \right) - \vec{\nabla} \cdot \delta \vec{F} + \vec{\xi} \cdot \vec{\nabla} (\vec{\nabla} \cdot \vec{F}_0) - \vec{\nabla} \cdot [(\vec{\xi} \cdot \vec{\nabla}) \vec{F}_0] \quad (3.6)$$

In what follows, we will neglect the Lagrangian perturbations to the energy production rate,  $\delta \epsilon$ .

The the energy flux can be separated into two main components:

$$\vec{F}_0 = \vec{F}_0^{\text{R}} + \vec{F}_0^{\text{C}} \quad (3.7)$$

where  $\vec{F}_0^{\text{R}}$  is the radiative energy flux, and  $\vec{F}_0^{\text{C}}$  the energy flux from convection. The radiative energy flux is given by the following relation:

$$\vec{F}_0^{\text{R}} = -\frac{4acT_0^3}{3\kappa_0\rho_0} \vec{\nabla} T_0 \quad (3.8)$$

where  $a$  is the radiation constant (deduced from the Stefan-Boltzmann constant),  $c$  the speed of light, and  $\kappa$  the Rosseland mean opacity. This equation can be perturbed as

follows:

$$\delta \vec{F}^{\text{R}} = \left[ 4 \frac{\delta T}{T_0} - \frac{\delta \kappa}{\kappa_0} - \frac{\delta \rho}{\rho_0} \right] \vec{F}_0^{\text{R}} - \frac{4acT_0^3}{3\kappa_0\rho_0} \left[ T_0 \vec{\nabla} \left( \frac{\delta T}{T_0} \right) + \vec{\xi} \cdot \vec{\nabla} \left( \vec{\nabla} T_0 \right) - \vec{\nabla} \left( \vec{\xi} \cdot \vec{\nabla} T_0 \right) \right] \quad (3.9)$$

In the frozen convection approximation, the Lagrangian perturbation to the convective energy flux is neglected:

$$\delta \vec{F}^{\text{C}} \simeq \vec{0} \quad (3.10)$$

Such an approximation neglects the interactions between pulsations and convections thus making it difficult to predict the red edge of the  $\delta$  Scuti instability strip due to the thin convective envelope present in these stars. A more realistic treatment such as time-dependent convection yields results in better agreement with observations (Dupret et al. 2004). However, such a treatment has not yet been implemented in the case of rapidly rotating stars.

Finally, the non-adiabatic equations are completed with perturbed equations of state and opacities. To this must be added various boundary conditions which ensure the solutions remain regular in the centre, the perturbations to the gravitational potential vanish at infinity, and the pressure and temperature variations take on the appropriate behaviour at the surface. More realistic surface conditions could be obtained if model stellar atmospheres were added onto the internal structure and a treatment similar to what is done in Dupret et al. (2003) carried out. However, this would imply using a grid of model atmospheres given that the effective temperature depends on latitude in rotating stars. This has yet to be implemented.

In the end, we end up with a generalised eigenvalue problem where the pulsation frequencies are the eigenvalues, and the various perturbations to equilibrium quantities correspond to the eigenvectors. In contrast to the non-rotating, spherically symmetric case, this problem is non-separable with respect to the radial coordinate,  $r$  or  $\zeta$ , and the co-latitude,  $\theta$ . However, there remains the symmetry with respect to the rotation axis, thereby allowing the  $\phi$  coordinate to be separated from the two other coordinates. Hence, this problem is two-dimensional and must be solved numerically as described in the following section.

### 3.2.2 Numerical implementation

The above system of equations is solved numerically in the Two-dimensional Oscillation Program (TOP, see Reese et al. 2006, 2009a). The numerical implementation can be broken down in two parts. The first part is the discretisation which transforms the above system of differential equations into matrix form. The second part corresponds to numerically solving this problem using a standard eigenvalue solver.

The first step in discretising the above system is expressing explicitly the equations in terms of a surface-fitting coordinate system such as the one illustrated in Fig. 3.1 for an ESTER model. The advantage of using surface-fitting coordinates is that it is possible to impose boundary conditions without loss of accuracy.

The equations are then projected onto the spherical harmonic basis. This is a two-step procedure. First the variables are expressed as sums of spherical harmonics. For instance,



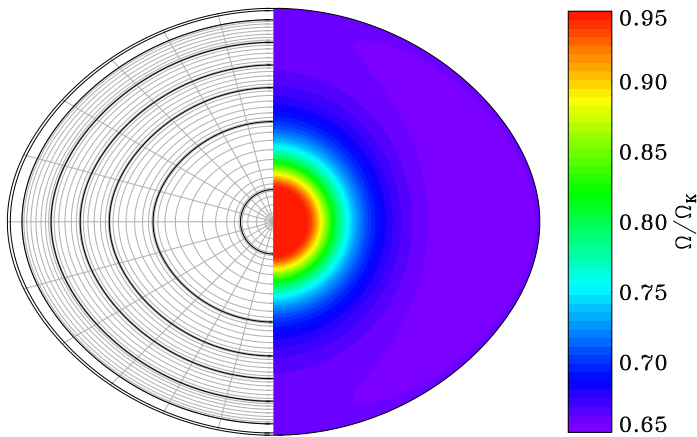


Figure 3.1: Coordinate system and rotation profile in an ESTER model (taken from Rieutord et al. 2016). ESTER models use a multi-domain approach as can be seen from the coordinate system. The rotation rates are indicated by the colour bar, where  $\Omega_K = \sqrt{GM/R_{\text{eq}}^3}$  is the Keplerian break-up rotation rate and  $R_{\text{eq}}$  the equatorial radius.

the perturbation to the gravitational potential becomes:

$$\Psi'(\zeta, \theta, \phi) = \sum_{\ell=|m|}^{\infty} \Psi_m^\ell(\zeta) Y_\ell^m(\theta, \phi) \quad (3.11)$$

where  $\zeta$  is the radial coordinate,  $\ell$  the harmonic degree,  $m$  the azimuthal order,  $\Psi_m^\ell$  a radial function, and  $Y_\ell^m$  a spherical harmonic. More complicated expressions also exist for vectorial quantities. Then, the product between the equations and various spherical harmonics are integrated over  $4\pi$  steradians. For the continuity equation, one would have:

$$\iint_{4\pi} \{\text{Continuity equation}\} (Y_{\ell'}^m)^* \sin\theta d\theta d\phi, \quad |m| \leq \ell' \leq \infty \quad (3.12)$$

where  $(.)^*$  denotes the complex conjugate. This leads to an infinite system of coupled 1D differential equations in terms of the radial variable  $\zeta$ , which is then truncated at some maximal value of  $\ell$  and  $\ell'$ . The coefficients which intervene in these equations are typically coupling integrals of the form:

$$C_{\ell\ell'}(\zeta) = \iint_{4\pi} G(\zeta, \theta) Y_\ell^m(\theta, \phi) [Y_{\ell'}^m(\theta, \phi)]^* \sin\theta d\theta d\phi \quad (3.13)$$

where  $G(\zeta, \theta)$  is typically a model-related or geometric function, and  $C_{\ell\ell'}(\zeta)$  the resultant coupling coefficient. These coupling integrals are calculated via Gauss-Legendre quadratures which are both efficient and accurate numerically.

Finally, the equations are discretised in the radial direction. For the sake of consistency, a similar discretisation is used in the pulsation calculations as in the models. For instance, in the case of SCF models, a finite-differences approach is used (Reese et al. 2009a, 2013) based on the numerically stable scheme described in Reese (2013). In ESTER models, a multi-domain spectral approach based on Chebyshev polynomials is used. In contrast to finite difference, one of the limitations of spectral approaches is that the grid is imposed beforehand for a given resolution thus hindering us from increasing the number of grid points where there are rapid spatial variations. The use of multiple domains bypasses this limitation by allowing us to introduce domains with a high resolution in the regions of the star where it is needed. A second advantage of the multi-domain approach is the

possibility of introducing true discontinuities in the stellar model and investigating their impact on stellar pulsations (Reese et al. 2011, 2014).

Once the problem has been discretised, it takes on the following form:

$$\mathcal{A}\vec{v} = \omega\mathcal{B}\vec{v} \quad (3.14)$$

where  $\mathcal{A}$  and  $\mathcal{B}$  are square matrices,  $\vec{v}$  the eigenmode, and  $\omega$  the eigenvalue (*i.e.* the pulsation frequency). In some cases, higher powers of the eigenvalue intervene. However, it is possible to rewrite the system so that it takes on the form given by Eq. (3.14) thanks to appropriate definitions of  $\mathcal{A}$ ,  $\mathcal{B}$ , and  $\vec{v}$ . This problem is solved for a few eigenmodes with the largest eigenvalues in terms of absolute value thanks to the Arnoldi-Chebyshev algorithm, in which the original system is approximated by a smaller matrix based on successive applications of the  $\mathcal{A}$  matrix to a starting vector. In order to calculate eigenvalues around a target value  $\sigma$ , the above problem can be rewritten using the following spectral transformation:

$$(\mathcal{A} - \sigma\mathcal{B})^{-1}\mathcal{B}\vec{v} = \mu\vec{v} \quad (3.15)$$

where  $\mu$  plays the role of an eigenvalue and  $\omega = \sigma + 1/\mu$ . As can be seen, solutions with large values of  $|\mu|$  are those which are closest to  $\sigma$ . Hence, applying the Arnoldi-Chebyshev algorithm to this modified version of the eigenvalue problem will yield the eigensolutions closest to  $\sigma$ .

An important contribution to the numerical cost is factoring the matrix  $\mathcal{A} - \sigma\mathcal{B}$ , a necessary step when applying  $(\mathcal{A} - \sigma\mathcal{B})^{-1}$ . In the case of SCF models,  $\mathcal{A} - \sigma\mathcal{B}$  has a band structure as a result of using finite differences. Efficient algorithms have been implemented within the linear algebra LAPACK library<sup>2</sup> in order to factor such matrices. When dealing with the multi-domain spectral ESTER models,  $\mathcal{A} - \sigma\mathcal{B}$  takes on a block tridiagonal structure. It is then possible to factorise only the diagonal blocks including some corrective terms rather than factorising the entire matrix. Once more, this reduces the amount of computation time and computer memory involved in the factorisation.

### 3.2.3 Variational principle and work integral

Once the pulsation frequencies have been calculated, it is possible to check their accuracy by means of an independent integral formula based on the associated eigenfunctions. This formula is obtained by taking the dot product of Euler's equation with the Lagrangian displacement multiplied by the equilibrium density and integrating this over the volume of the star:

$$\iiint_V \rho_0 \vec{\xi}^* \cdot \{\text{Euler's equation}\} dV \quad (3.16)$$

where  $a^*$  denotes the complex conjugate of  $a$ . After a lengthy derivation, one obtains an equation of the form (Reese et al. in prep):

$$A\omega^2 + 2B\omega + C = 0 \quad (3.17)$$

---

<sup>2</sup>See <http://www.netlib.org/lapack/>.

where  $A$  and  $B$  are real, and  $C$  and  $\omega$  are complex. Explicit expressions for  $A$ ,  $B$ , and  $C = C_R + iC_I$  are:

$$A = \int_V \rho_0 \xi^2 dV, \quad (3.18)$$

$$B = \int_V \rho_0 \left[ m\Omega \xi^2 - i\vec{\Omega} \cdot (\vec{\xi} \times \vec{\xi}^*) \right] dV, \quad (3.19)$$

$$\begin{aligned} C_R = & \int_V \left\{ (m^2 + 1) \rho_0 \Omega^2 \xi^2 - 2im\rho_0 \Omega \vec{\Omega} \cdot (\vec{\xi} \times \vec{\xi}^*) - \rho_0 \left| \vec{\Omega} \cdot \vec{\xi} \right|^2 - \vec{\xi}^* \cdot \left[ \vec{\xi} \cdot \vec{\nabla} (\vec{\nabla} P_0) \right] \right. \\ & \left. - \rho_0 \vec{\xi}^* \cdot \left[ \vec{\xi} \cdot \vec{\nabla} (\vec{\nabla} \Psi_0) \right] + \Re \left\{ -\frac{\delta P \delta \rho^*}{\rho_0} + 2 \left( \vec{\xi} \cdot \vec{\nabla} P_0 \right) \frac{\delta \rho^*}{\rho_0} \right\} \right\} dV \\ & + \sum_i \int_{S_i} \vec{\xi} \cdot (\vec{\nabla} P_0^- - \vec{\nabla} P_0^+) \vec{\xi}^* \cdot d\vec{S} - \int_S \Re \left\{ \delta P \vec{\xi}^* \cdot d\vec{S} \right\} + \int_{V_\infty} \frac{\|\vec{\nabla} \Psi'\|^2}{4\pi G} dV, \end{aligned} \quad (3.20)$$

$$C_I = - \int_V \Im \left\{ \frac{\delta P \delta \rho^*}{\rho_0} \right\} dV - \int_S \Im \left\{ \delta P \vec{\xi}^* \cdot d\vec{S} \right\}, \quad (3.21)$$

where we've dropped the triple integral notation,  $\xi = \|\vec{\xi}\|$ ,  $V$  is the stellar volume,  $V_\infty$  infinite space (including the star),  $S$  the stellar surface,  $S_i$  the surfaces of any discontinuity that may be present in the model (including the surface),  $P_0^-$  the pressure right below the discontinuity, and  $P_0^+$  the pressure right above. We note that the surface element vectors  $d\vec{S}$  are always orientated outwards. When discontinuities are present, the volume integrals are to be understood as the sum of the volume integrals over the domains delimited by the discontinuities - the surface terms given above deal with the transitions from one domain to the next. Solving Eq. (3.17) leads to the following relations:

$$\omega_R = -\frac{B}{A} \pm \sqrt{\frac{B^2 - AC_R + \sqrt{(B^2 - AC_R)^2 + A^2 C_I^2}}{2A^2}} \quad (3.22)$$

$$\omega_I = -\frac{C_I}{2(A\omega_R + B)} \quad (3.23)$$

where  $\omega = \omega_R + i\omega_I$ . We note that  $\omega_I$  is the damping rate - positive values of  $\omega_I$  correspond to mode damping. The larger of the two solutions of Eq. (3.22) corresponds to the pulsation frequency, and Eq. (3.23) is the work integral.

When adiabatic calculations are carried out, the above expressions simplify. Indeed, the adiabatic relation  $\delta P/P_0 = \Gamma_1(\delta\rho/\rho_0)$  can be used to simplify various terms in Eq. (3.20), and causes  $\delta P$  and  $\delta\rho$  to be in phase thus cancelling out the first term in Eq. (3.21). Furthermore, both the real and imaginary parts of  $\int_S \delta P \vec{\xi}^* \cdot d\vec{S}$  vanish if one applies the boundary condition  $\delta P = 0$  as is typical in adiabatic calculations. Hence, the term  $C_I$  vanishes entirely thus leading to  $\omega_I = 0$  if one applies Eq. (3.23) - alternate expressions of the work integral would lead to non-zero values of  $\omega_I$ , in particular when

applying the quasi-adiabatic approximation. The simplified expression for  $C_R$  is:

$$\begin{aligned}
C_R = & \int_V \left\{ (m^2 + 1) \rho_0 \Omega^2 \xi^2 - 2im\rho_0 \Omega \vec{\Omega} \cdot (\vec{\xi} \times \vec{\xi}^*) - \rho_0 \left| \vec{\Omega} \cdot \vec{\xi} \right|^2 - \vec{\xi}^* \cdot \left[ \vec{\xi} \cdot \vec{\nabla} \left( \vec{\nabla} P_0 \right) \right] \right. \\
& \left. - \rho_0 \vec{\xi}^* \cdot \left[ \vec{\xi} \cdot \vec{\nabla} \left( \vec{\nabla} \Psi_0 \right) \right] - \frac{|P'|^2}{\Gamma_1 P_0} + \frac{|\vec{\xi} \cdot \vec{\nabla} P_0|^2}{\Gamma_1 P_0} \right\} dV \\
& + \sum_i \int_{S_i} \vec{\xi} \cdot \left( \vec{\nabla} P_0^- - \vec{\nabla} P_0^+ \right) \vec{\xi}^* \cdot d\vec{S} + \int_{V_\infty} \frac{\|\vec{\nabla} \Psi'\|^2}{4\pi G} dV
\end{aligned} \tag{3.24}$$

It is important to note that in the adiabatic case, the pulsation equations are symmetric with respect to the dot product defined in Eq. (3.16). This leads to the variational principle which states that to first order, errors on the eigenfunctions do not affect the frequency obtained via Eq. (3.22) (Lynden-Bell & Ostriker 1967). Hence, this “variational frequency” can be used as a more accurate estimate of the pulsation frequency (*e.g.* Christensen-Dalsgaard et al. 1979).

### 3.3 Mode classification

Having described how pulsation modes are calculated in rapidly rotating stars, we can now turn our attention to some of the results which have been obtained over the past few years. I start by describing the classification of modes in the presence of rapid rotation as this is important for understanding the ensuing discussions as well as the various issues at stake. I will first describe acoustic modes before dealing with gravito-inertial modes.

#### 3.3.1 Acoustic modes

At the high end of the pulsation frequency spectrum are acoustic modes. These are modes for which the restoring force is pressure. When rotation is present, these modes are affected by the centrifugal deformation, and to a lesser degree by the Coriolis force. Using ray dynamics, Lignières & Georgeot (2008, 2009), showed that at rapid rotation rates, acoustic modes subdivide into different classes of pulsation modes, each characterised by a specific geometry and an independent frequency organisation. These classes include: 2-period island modes, chaotic modes, 6-period island modes, and whispering gallery modes. These modes are the rotating counterparts to modes with low, low-intermediate, high-intermediate, and high values of  $\ell - |m|$  respectively, where  $\ell$  is the harmonic degree,  $m$  the azimuthal order, and  $\ell - |m|$  the number of nodal lines parallel to (and including) the equator. The term “island mode” derives from the Poincaré surface of section for which the region occupied by island modes corresponds to regular island within chaotic regions.

This classification was initially derived for polytropic stellar models but later extended to the more realistic SCF models based on mode geometry (Reese et al. 2009a) and is also present in ESTER models. Figure 3.2 illustrates the meridional cross-section of pulsation modes from 3 of these classes. In some of the SCF models with extreme differential rotation, some of these classes of modes seem to disappear, as described in Reese et al. (2009a), but may reappear at large values of  $|m|$ .

Of these different classes of modes, island modes are the most interesting. Indeed, these are the most visible in terms of disc-integrated observations (Lignières & Georgeot

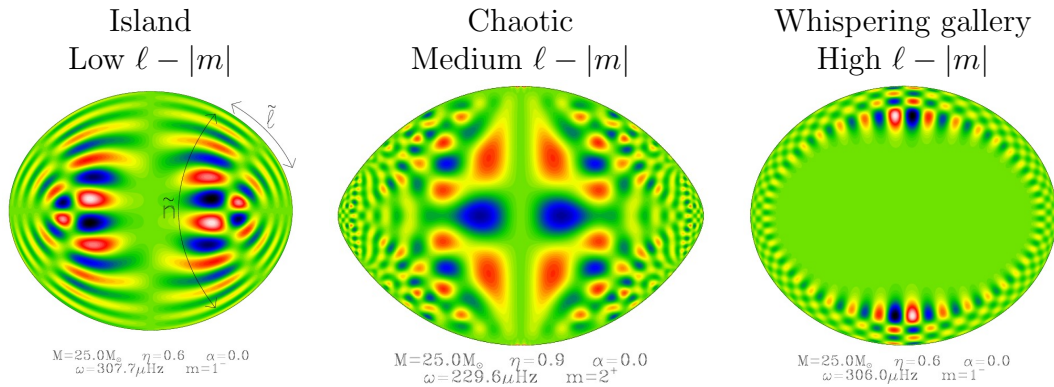


Figure 3.2: Different classes of acoustic modes in rapidly rotating stars (taken from Reese et al. 2009a).

2009, Reese et al. 2013) and their frequencies follow a regular pattern as will be described in Sect. 3.4. Furthermore, these modes are described by new quantum numbers which are illustrated in the left panel of Fig. 3.2.  $\tilde{n}$  is the number of nodes along the underlying ray path and  $\tilde{\ell}$  gives the number of node lines parallel to the underlying ray path. To these must be added  $m$  the azimuthal order which retains the same definition as in the non-rotating case. A relationship based on “node conservation” between the usual spherical quantum numbers ( $n, \ell$ ) and the island mode quantum numbers can be derived:

$$\left\{ \begin{array}{l} \tilde{n} = 2n + \varepsilon \\ \tilde{\ell} = \frac{\ell - |m| - \varepsilon}{2} \\ \varepsilon = \ell + m \pmod{2} \end{array} \right. \quad \left\{ \begin{array}{l} n = \frac{\tilde{n} - \varepsilon}{2} \\ \ell = 2\tilde{\ell} + |m| + \varepsilon \\ \varepsilon = \tilde{n} \pmod{2} \end{array} \right. \quad (3.25)$$

where  $\varepsilon$  corresponds to mode parity (*i.e.*  $\varepsilon = 0$  if the mode is symmetric with respect to the equator and  $\varepsilon = 1$  when it is antisymmetric). It is hoped that a successful identification of these modes will lead to detailed seismic constraints on the structure of rapidly rotating acoustic oscillators.

### 3.3.2 Gravito-inertial modes

At the low end of the frequency spectrum are gravity modes for which the restoring force is buoyancy. When rotation rate is present, these modes are affected by the Coriolis force, and to a lesser degree by the centrifugal deformation. Given that the Coriolis force combines with buoyancy, we will call these gravito-inertial modes. We note that some modes, such as r-modes, owe their existence to the Coriolis force and are therefore called inertial modes (*e.g.* Papaloizou & Pringle 1978, Rieutord et al. 2001, Lee 2006). In what follows, however, we will restrict our attention to modes which are the rotating counterparts to gravity modes.

Various detailed classifications of these modes have been proposed in the past (see, *e.g.* Townsend 2003b, and references therein). However, in what follows, we will give a somewhat simpler and less detailed classification. Gravito-inertial modes can be subdivided into two categories: sub-inertial modes for which  $\omega < 2\Omega$ , and super-inertial modes for which  $\omega > 2\Omega$ . In the sub-inertial regime, a critical latitude appears which confines the

modes to equatorial regions (*e.g.* Dintrans & Rieutord 2000, Townsend 2003b, Ballot et al. 2010). In the super-inertial regime, the geometric structure of the modes changes very little compared to the non-rotating case. An exception to this rule is the so-called rosette modes, discovered by Ballot et al. (2012). These modes take on a distinct geometric rosette-like pattern which closely matches the underlying ray paths. Their non-separable structure means that they cannot be correctly described with the traditional approximation, a popular approach for calculating gravito-inertial modes. However, a perturbative analysis including the effects of near degeneracies can reproduce their structure (Takata & Saio 2013, Saio & Takata 2014). Figure 3.3 displays the meridional cross-section of modes from these different categories.

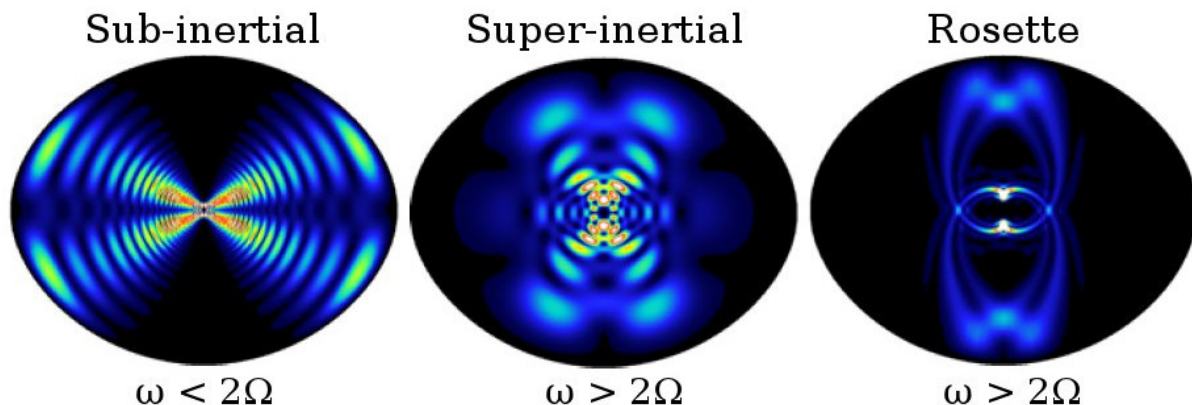


Figure 3.3: Different types of gravito-inertial modes in rapidly rotating stars (taken from Ballot et al. 2013).

We note that Prat et al. (2018) recently investigated pulsations in differentially rotating stars using ray dynamics. They find ray trajectories which represent new classes of modes, in particular the trans-inertial modes for which the pulsation frequency lies in the interval  $[2 \min(\Omega), 2 \max(\Omega)]$ . Numerical calculations using a two-dimensional pulsation code such as TOP will be needed to find eigenmodes which are the counterparts to these ray trajectories.

### 3.4 Frequency patterns

As was mentioned in the previous chapter, frequency patterns are typically used in solar-like (and hence slowly rotating) pulsators to identify modes. In the rapidly rotating case, using frequency patterns to identify modes is not so straightforward. Indeed, rotation considerably complicates the frequency spectrum of such stars. This is furthermore compounded by the fact that there is currently no theory fully capable of predicting mode amplitudes in such stars. Nonetheless, it is important to study frequency patterns, both from a theoretical and an observational point of view, as this is sometimes the only seismic information available.

In what follows, we will focus our attention on the frequencies of island modes. We note that considerable work has gone into studying the pulsation frequencies of gravito-inertial modes using both the traditional approximation (*e.g.* Berthomieu et al. 1978, Lee & Saio 1987, Bouabid et al. 2013) and full 2D calculations (*e.g.* Ballot et al. 2010, Ouazzani et al.

2017). Also, Lignières & Geogteot (2009) looked at the frequency organisation of chaotic and whispering gallery modes in addition to that of the island modes. Current work based on techniques from quantum chaos is investigating the distribution and frequency separations of chaotic acoustic mode frequencies (Evano et al., in prep.).

### 3.4.1 An asymptotic formula for island modes

Initially, Lignières et al. (2006) obtained an empirical formula describing the frequencies of axisymmetric island modes in polytropic stellar models. This formula is analogous to the asymptotic formula from Tassoul (1980) except that the ratio between the large frequency separation,  $\Delta_n = \omega_{n+1, \ell, m} - \omega_{n, \ell, m}$ , and the spacing for consecutive  $\ell$  values,  $\Delta_\ell$ , is not necessarily two but depends on the rotation rate. This formula was subsequently extended to non-axisymmetric by Reese et al. (2008) who also showed that  $\Delta_n$  continues to scale with the square-root of the stellar mean density, even at high rotation rates, as illustrated in Fig. 3.4.

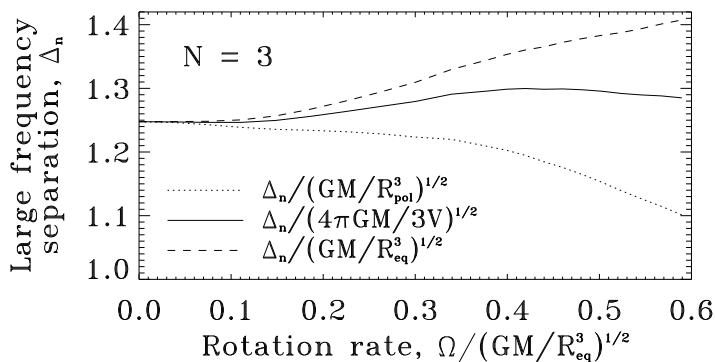


Figure 3.4: Large frequency separation as a function of the rotation rate for an  $N = 3$  polytrope. The large frequency separation has been normalised by the square-root of different calculations of the mean density involving the true volume and the volume based on the equatorial or polar radii (taken from Reese et al. 2008).

In the mean time, Lignières & Geogteot (2008) used ray dynamics to justify the empirical formula from Lignières et al. (2006) and demonstrate its asymptotic nature. This analysis was extended to non-axisymmetric modes by Lignières & Geogteot (2009). In these articles, they showed that the frequency separation between modes with consecutive  $\tilde{n}$  values,  $\Delta_{\tilde{n}}$  (*i.e.* half the large frequency separation – see Eq. 3.25), is simply half of the inverse acoustic travel time along the underlying ray trajectory. They also tested this relation numerically and found it to be accurate to within 2.2%. They found a preliminary formula for  $\Delta_{\tilde{\ell}} = \omega_{\tilde{n}, \tilde{\ell}+1, m} - \omega_{\tilde{n}, \tilde{\ell}, m}$ , formula which was later extended by Pasek et al. (2011, 2012) and tested through comparisons with pulsation calculations using TOP.

Reese et al. (2009a) showed that the above empirical formula also applies in more realistic models, namely the SCF models, as did subsequent works (Reese et al. 2014, Ouazzani et al. 2015b). The behaviour of the frequencies at high values of  $|m|$  and  $\tilde{n}$  was investigated, thus leading to the following empirical formula<sup>3</sup>:

$$\omega_{\tilde{n}, \tilde{\ell}, m} \simeq \tilde{n} \Delta_{\tilde{n}} + D_m(\tilde{\ell}) \sqrt{\frac{m^2}{\tilde{n}} + \mu(\tilde{\ell})^2} - m\Omega + \alpha(\tilde{\ell}) \quad (3.26)$$

<sup>3</sup>This formula is written for the retrograde convention, where positive  $m$  values correspond to retrograde modes.

Pasek et al. (2012) also found a dependence of the form  $m/\sqrt{\tilde{n}}$  for non-axisymmetric modes based on ray theory. The left panel of Fig. 3.5 illustrates a frequency spectrum for a uniformly rotating SCF model which has been fitted using a slightly simplified version of Eq. (3.26). The right panel superimposes several sequences of island mode frequencies as a function of  $m/\sqrt{\tilde{n}}$  for large values of  $\tilde{n}$ .

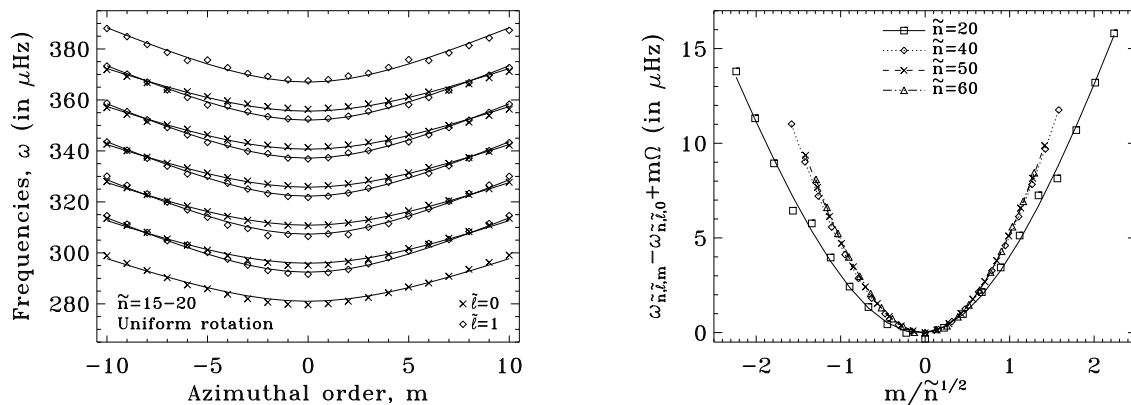


Figure 3.5: Spectrum of corotating pulsation frequencies (*i.e.* without the advective term  $-m\Omega$ ) for  $\tilde{n} = 15 - 20$  and  $\tilde{\ell} = 0 - 1$  (left panel), and scaled frequency sequences for  $\tilde{n} = 20, 40, 50$  and  $60$  and  $\tilde{\ell} = 0$  (right panel) in a  $25 M_{\odot}$  SCF model rotating at  $0.6 \Omega_K$  (taken from Reese et al. 2009a).

Of particular interest is the generalised rotational splitting, defined as:

$$S_m = \frac{\omega_{\tilde{n}, \tilde{\ell}, -m} - \omega_{\tilde{n}, \tilde{\ell}, m}}{2m} \quad (3.27)$$

Based on Eq. (3.26), it turns out that  $S_m \simeq \Omega$  much like in the slowly rotating case. This, however, neglects the effects of the Coriolis force as well as those of differential rotation when present. To go beyond these limitations, one can derive the following relation based on the variational principle and using various approximations (Reese et al. 2009a, in prep.), provided the differential rotation is not too strong:

$$S_m \simeq \frac{\Omega_m^{\text{eff}} + \Omega_{-m}^{\text{eff}}}{2} + \frac{\mathcal{C}_m + \mathcal{C}_{-m}}{2} \quad (3.28)$$

where

$$\Omega_{\text{eff}} = \frac{\int_V \Omega \rho_o \|\vec{\xi}\|^2 dV}{\int_V \rho_o \|\vec{\xi}\|^2 dV} \quad (3.29)$$

$$\mathcal{C} = \frac{i \int_V \rho_o \vec{\Omega} \cdot (\vec{\xi}^* \times \vec{\xi}) dV}{m \int_V \rho_o \|\vec{\xi}\|^2 dV} \quad (3.30)$$

The left panel of Fig. 3.6 compares the generalised rotational splitting with the integral formula for a selection of modes in a  $3 M_{\odot}$  ESTER model rotating at  $0.7 \Omega_K$ . The right-hand side of Eq. (3.28) is of the form  $\frac{1}{2} \int_V (K_{\tilde{n}, \tilde{\ell}, m}(\zeta, \theta) + K_{\tilde{n}, \tilde{\ell}, -m}(\zeta, \theta)) \Omega(\zeta, \theta) dV$  where



the  $K$  functions are rotation kernels. The right panel of Fig. 3.6 illustrates one such kernel. It is an open question whether the accuracy of Eq. (3.28) is sufficient to allow the use of inverse methods to probe the rotation profile, provided a sufficient number of island modes are identified.

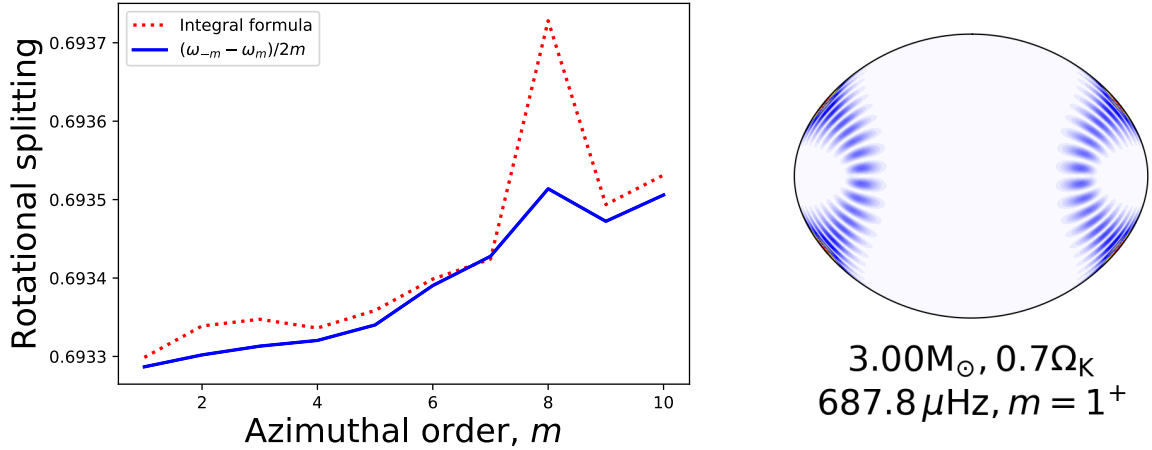


Figure 3.6: (Left) Generalised rotational splittings vs. integral formula for a selection of modes in a 3 M<sub>⊙</sub> ESTER model rotating at 0.7 Ω<sub>K</sub>. (Right) The rotational kernel for the mode at  $m = 1$ .

### 3.4.2 Interpreting observations

Various works then investigated whether it is possible to exploit the frequency patterns present in the island mode frequencies when interpreting observed pulsation spectra. For instance, Lignières et al. (2010) created artificial pulsation spectra using the island mode asymptotic formula for the frequencies, and mode visibilities based on the disc integrated visibilities from Lignières & Georgeot (2009). They then showed it was possible to extract recurrent frequency spacings such as  $2\Omega$  and sometimes  $\Delta_n$  from the autocorrelation function of the frequency spectrum, depending on the inclination and the frequency range of the spectrum. This was followed by Reese et al. (2017b) who worked with pulsation spectra from SCF models at various rotation rates instead of asymptotic frequencies, and used more realistic mode visibilities based on Reese et al. (2013) (see following section). In this work, the autocorrelation function of the frequency spectrum was investigated as was its Fourier transform, thus showing that it may be possible to identify the large frequency separation, half its value, and  $2\Omega$  depending on the inclination and number of modes in the spectrum, and assuming a regular behaviour for the intrinsic mode amplitudes (which are then subsequently multiplied by the mode visibilities). If, however, random intrinsic amplitudes are used, it becomes quite difficult to reliably identify the above spacings, except in some cases for models rotating at  $0.3\Omega_K$  and  $0.7\Omega_K$  for which  $2\Omega$  coincides with  $\Delta_{\bar{n}} = \Delta_n/2$  and  $\Delta_n$ , respectively, as illustrated in Fig. 3.7.

On the observational side, various authors found recurrent spacings or patterns in  $\delta$  Scuti stars. For instance, thanks to Fourier transforms of the frequency spectrum of a star observed by CoRoT, García Hernández et al. (2009) found a recurrent spacing which they interpreted as half the large frequency separation (see left panel of Fig. 3.8). Others

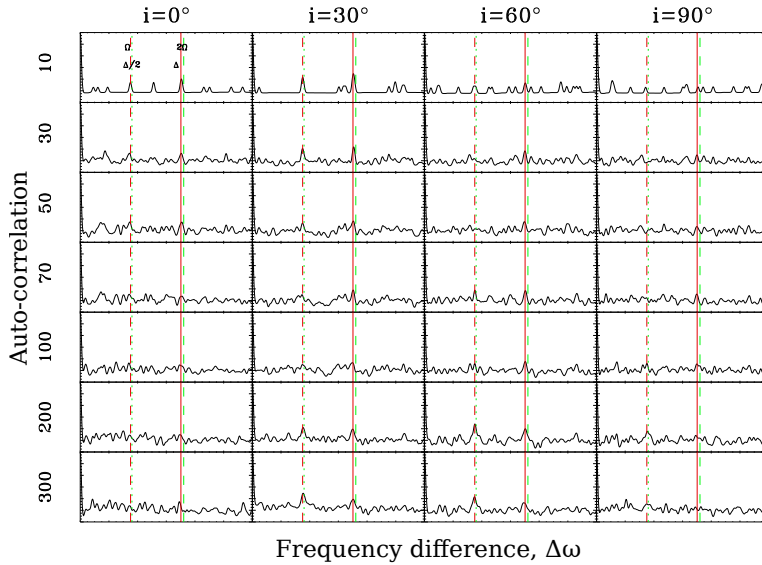


Figure 3.7: Autocorrelation functions of frequency spectra with random intrinsic amplitudes between 1 and 100 for an SCF model rotating at  $0.7\Omega_K$  for different inclinations (columns) and number of selected modes (rows). Once the highest amplitude modes are selected their amplitudes are set to a constant value prior to calculating the autocorrelation function.

(Mantegazza et al. 2012, García Hernández et al. 2013, 2015, 2017, Paparó et al. 2016a,b, Michel et al. 2017), using power spectra or Fourier transforms of frequency distributions, histograms of frequency differences, echelle diagrams, visual inspection, and comparisons between multiple pulsation spectra, found recurrent spacings and patterns in observed frequency spectra. Of particular interest is the work by García Hernández et al. (2015), in which it was shown that the recurrent spacings in a selection of  $\delta$  Scuti stars in binary systems scale with the root mean densities obtained by independent means regardless of the rotation rate (see right panel of Fig. 3.8), in accordance with the predictions from Reese et al. (2008) and more recent calculations based on SCF models. This was followed by García Hernández et al. (2017), who estimated  $\log(g)$ , using mean densities obtained from frequency spacings and parallaxes from Hipparcos or Gaia, and found a good agreement with  $\log(g)$  values from binary analysis.

Reese et al. (2009b) proposed a strategy for identifying individual modes which consisted in scanning the parameter space formed by the coefficients of the asymptotic formula to find best matching spectra for a given set of observed frequencies. This method works well in the absence of chaotic modes, or at very high radial orders. However, as based on the visibility calculations of Lignières & Georgeot (2009), Reese et al. (2013), chaotic modes are expected to be visible. Furthermore, the radial mode orders in  $\delta$  Scuti stars are expected to be lower both observationally (Michel et al. 2017) and theoretically (Dupret et al. 2004)). What is therefore needed is a systematic study of a grid of rotating stellar models, analogous to the study carried out by Suárez et al. (2014) for non-rotating  $\delta$  Scutis, to further constrain the behaviour of the coefficients in the asymptotic formula and hence restrict the associated parameter space. In parallel, observational mode identification strategies, such as what is described in the next section, need to be developed.

### 3.5 Mode identification techniques

Observational mode identification techniques rely on exploiting various observational indications which constrain the geometry of the underlying modes. These can include line

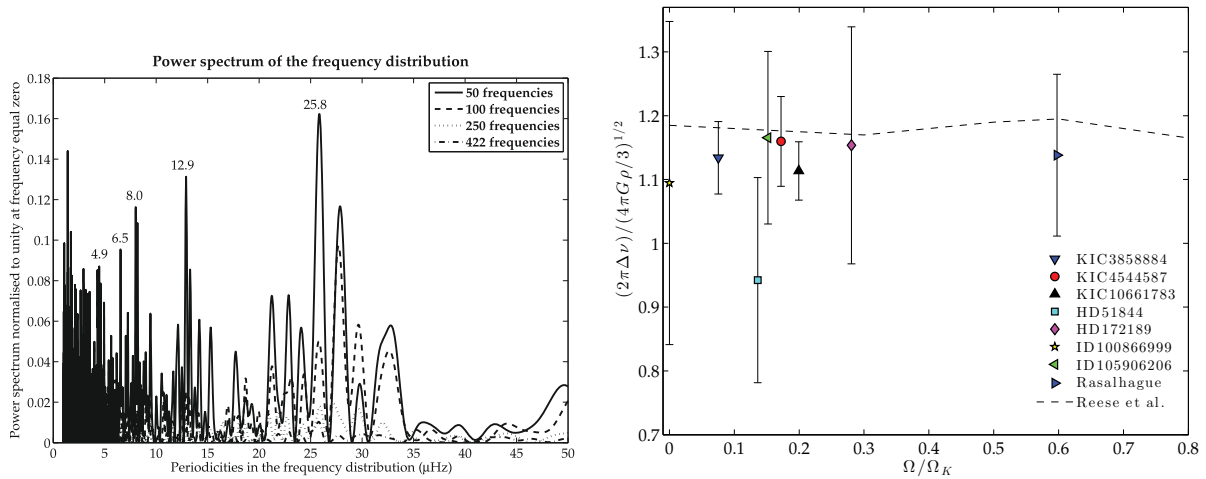


Figure 3.8: (Left) Fourier transform of various selections of observed frequencies in a  $\delta$  Scuti star observed by CoRoT (taken from García Hernández et al. 2009). (Right): ratio between recurrent frequency spacings, interpreted as the large separation, and root mean densities, as a function of the rotation rate (taken from García Hernández et al. 2015).

profile variations (LPVs) which result from Doppler shifts induced by the pulsation velocity fields, or comparisons of pulsation amplitudes and phases in various photometric bands (*e.g.*, Chapter 6 of Aerts et al. 2010). These have been a popular technique for main sequence massive and intermediate mass stars, excited by the classical  $\kappa$ -mechanism. However, much work is still needed in order to adapt these techniques to rapid rotators. The following sections describe these techniques in more detail as well as some of the latest efforts to include the effects of rapid rotation.

### 3.5.1 Multicolour mode visibilities

Multicolour mode identification consists in observing pulsation modes in different photometric bands, calculating the ratio between the amplitudes in the different bands as well as the phase differences, and comparing these to theoretical predictions. The advantage of doing this is that the amplitude ratios and the phase differences do not depend on the intrinsic mode amplitude, but only on its geometric characteristics. Hence, a linear pulsation code can provide realistic predictions for such quantities based on mode visibilities in different photometric bands. Furthermore, in the non-rotating case, these do not depend on the azimuthal order or the inclination of the star, thereby facilitating the comparison with theoretical expectations.

Various authors have looked into including the effects of rotation in amplitude ratios and phase differences. For instance, Daszyńska-Daszkiewicz et al. (2002), Daszyńska-Daszkiewicz et al. (2007) and Townsend (2003a) have carried out realistic mode visibility calculations (including non-adiabatic effects) but approximated the effects of rotation (either by using a perturbative approach or the traditional approximation). This allowed them to show that amplitude ratios and phase differences depend on the azimuthal order and the stellar inclination in the rotating case. Savonije (2013) carried out slightly simplified visibility calculations while fully including the effects of the Coriolis acceleration

as well as non-adiabatic effects, but neglecting the centrifugal deformation. In contrast, Lignières et al. (2006), Lignières & Georgeot (2009) calculated disk integration factors (*i.e.*, a simplified version of mode visibilities) but fully including the effects of rotation in the pulsation calculations. They showed that chaotic acoustic modes are expected to be more visible than their non-rotating counterparts and may need to be taken into account when interpreting observed pulsation spectra. Reese et al. (2013) carried out realistic mode visibility calculations while fully including the effects of rotation, but neglected or approximated non-adiabatic effects. Finally, Reese et al. (2018) fully included non-adiabatic effects in realistic mode visibility calculations.

In order to calculate the variations of light in a pulsating star in a particular photometric band, one must first express the radiated energy of a non pulsating star received by an observer per unit of time and unit of detector surface:

$$E = \frac{1}{d^2} \iint_{\text{Vis.Surf.}} I(\mu, g_{\text{eff}}, T_{\text{eff}}) \vec{e}_{\text{obs.}} \cdot d\vec{S} \quad (3.31)$$

where  $d$  is the distance between the observer and the star, “Vis. Surf.” the visible surface (*i.e.* made up of the surface elements pointing to the observer),  $I(\mu, g_{\text{eff}}, T_{\text{eff}})$  the specific radiation intensity in the relevant photometric band (as deduced, for instance, from model atmospheres),  $\mu$  the cosine of the angle between the line of sight and the outward normal to the surface,  $g_{\text{eff}}$  the effective gravity (including the centrifugal acceleration),  $T_{\text{eff}}$  the effective temperature,  $\vec{e}_{\text{obs.}}$  the vector pointing to the observer, and  $d\vec{S}$  the vectorial surface element. We note the above expression is only valid for stars with a convex shape. If the star is concave (as can be the case for some of the SCF models with extreme differential rotation – see, *e.g.*, Jackson et al. 2004), certain parts of the surface may be hidden by other parts, thus requiring the use of a ray tracing method.

When the star is pulsating, this quantity is perturbed as follows:

$$\begin{aligned} \Delta E(t) = & \frac{1}{d^2} \Re \left\{ \iint_{\Delta(\text{Vis.Surf.})} I(\mu, g_{\text{eff}}, T_{\text{eff}}) \vec{e}_{\text{obs.}} \cdot d\vec{S} \right. \\ & + \iint_{\text{Vis.Surf.}} \delta I(\mu, g_{\text{eff}}, T_{\text{eff}}, t) \vec{e}_{\text{obs.}} \cdot d\vec{S} \\ & \left. + \iint_{\text{Vis.Surf.}} I(\mu, g_{\text{eff}}, T_{\text{eff}}) \vec{e}_{\text{obs.}} \cdot \delta(d\vec{S}) \right\} \end{aligned} \quad (3.32)$$

where  $\Re\{\dots\}$  denotes the real part of some quantity, and  $\Delta(\text{Vis.Surf.})$  the perturbation to the visible surface (given that the outward normal at each point is perturbed by the pulsations). It turns out that the first term in Eq. (3.32) is of the order of the square of the perturbation, hence it is negligible. The second term is developed using the following relation:

$$\delta I = I \left( \frac{\partial \ln I}{\partial \ln T_{\text{eff}}} \frac{\delta T_{\text{eff}}}{T_{\text{eff}}} + \frac{\partial \ln I}{\partial \ln g_{\text{eff}}} \frac{\delta g_{\text{eff}}}{g_{\text{eff}}} \right) + \frac{\partial I}{\partial \mu} \delta \mu \quad (3.33)$$

where the terms  $\partial \ln I / \partial \ln T_{\text{eff}}$ ,  $\partial \ln I / \partial \ln g_{\text{eff}}$ , and  $\partial I / \partial \mu$  are deduced from model atmospheres, and the terms  $\delta T_{\text{eff}} / T_{\text{eff}}$ ,  $\delta g_{\text{eff}} / g_{\text{eff}}$ , and  $\delta \mu$  from stellar pulsations. Detailed expressions as well as a complete derivation of this latter group of terms including the effects of rapid differential rotation is provided in Reese et al. (2013). It is important

to note that  $\delta T_{\text{eff}}/T_{\text{eff}}$  can only be obtained accurately through non-adiabatic pulsation calculations. For completeness, one would also have to include the effects of a Doppler shift in  $\delta I$  as this shifts the intensity profile as a function of wavelength thereby slightly modifying the received energy, whether integrated over the relevant range associated with the broadband filter or over the entire spectrum. However, this effect is probably not very important for mode visibilities. Finally, the perturbed surface element which appears in the third term is developed as follows:

$$\delta(d\vec{S}) = \delta(\partial_\theta \vec{r} \times \partial_\phi \vec{r}) d\theta d\phi = \left( \partial_\theta \vec{\xi} \times \partial_\phi \vec{r} + \partial_\theta \vec{r} \times \partial_\phi \vec{\xi} \right) d\theta d\phi \quad (3.34)$$

Figure 3.9 illustrate these different contributions to  $\Delta E(t)$ . Figure 3.10 then shows the sort of amplitude ratios and phase differences which can be obtained in the Geneva and BRITE photometric systems. As can be seen from the left panel, modes with the same  $\ell$  and  $m$  values can have similar amplitude ratios, even at rapid rotation rates. Based on this observation, Reese et al. (2017b) suggested grouping together modes with similar amplitude ratios in the hopes of forming families of modes with similar quantum numbers. Figure 3.11 shows one such grouping of modes with similar amplitude ratios. As can be seen, a number of these modes are island modes with similar quantum numbers. Studying their distribution of frequencies may then reveal characteristic frequency spacings from the asymptotic formula and constrain mode identification. An alternate approach consists in carrying out a  $\chi^2$  minimisation of the differences between observed amplitude ratios and phase difference and theoretical expectations (*e.g.* Daszyńska-Daszkiewicz et al. 2015).

### 3.5.2 Line profile variations

A complementary approach to photometric mode identification is exploiting line profiles variations (LPVs). As briefly explained above, the velocity field from the pulsations and the stellar rotation locally shift spectroscopic absorption lines due to the Doppler effect. When integrated over the visible disc, this leads to an enlarged absorption line which furthermore changes shape as the pulsation velocity field varies with time. Unlike amplitude ratios and phase differences, LPVs depend on the intrinsic mode amplitudes. Nonetheless, the information content in LPVs is quite rich, and can thus provide constraints on the underlying mode geometry and associated quantum numbers.

In order to calculate LPVs, one needs to start with essentially the same equation as Eq. (3.32) but include the dependence on wavelength as well as the Doppler shifts resulting from the pulsation velocity field. As the mode phase varies with time, the resultant LPVs will also vary.

Relatively few articles have dealt with the effects of rapid rotation on LPVs. Clement (1994) obtained LPVs for g-modes calculated with his 2D pulsation code. Relatively little detail is given on the ingredients which went into the LPV calculation. Later on, Townsend (1997) used the traditional approximation to calculate the effects of rapid rotation on stellar pulsations, then proceeded to calculate rather realistic LPVs. Reese et al. (2017a) provide some examples of LPV calculations based on non-adiabatic modes in an ESTER model (also see Fig. 3.12). These calculations use a number of simplifying assumptions: a blackbody spectrum is used to model the continuum and include the effects of gravity darkening, a crude limb-darkening law is used, the intrinsic line profile (prior to including Doppler shifts) is Gaussian, and any temperature-dependence of line

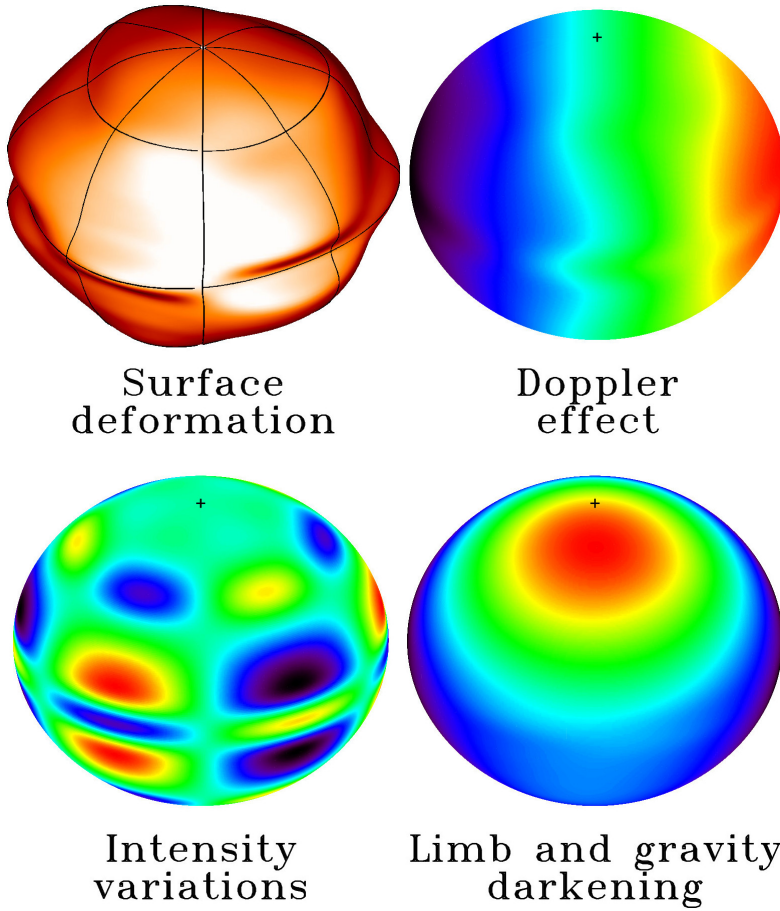


Figure 3.9: Different contributions to mode visibilities and line profile variations. We note that the stellar deformation includes both the centrifugal deformation and the deformation resulting from the pulsations (which is greatly exaggerated here), and that the Doppler shifts include the contributions from both the stellar rotation and the pulsations.

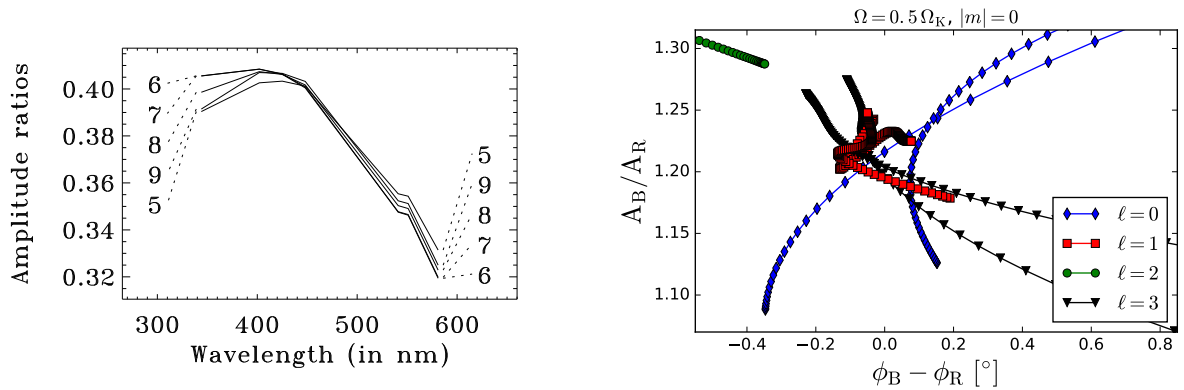


Figure 3.10: (Left) Amplitude ratios in the Geneva photometric system for a series adiabatic modes with the same  $\ell$  and  $m$  values, but consecutive  $n$  values, in a  $2 M_\odot$  SCF model at  $0.8 \Omega_K$  (taken from Reese et al. 2013). (Right) Amplitude ratios vs. phase differences in the BRIDE photometric system for non-adiabatic modes in a  $9 M_\odot$  ESTER model at  $0.5 \Omega_K$  (taken from Reese et al. 2018).

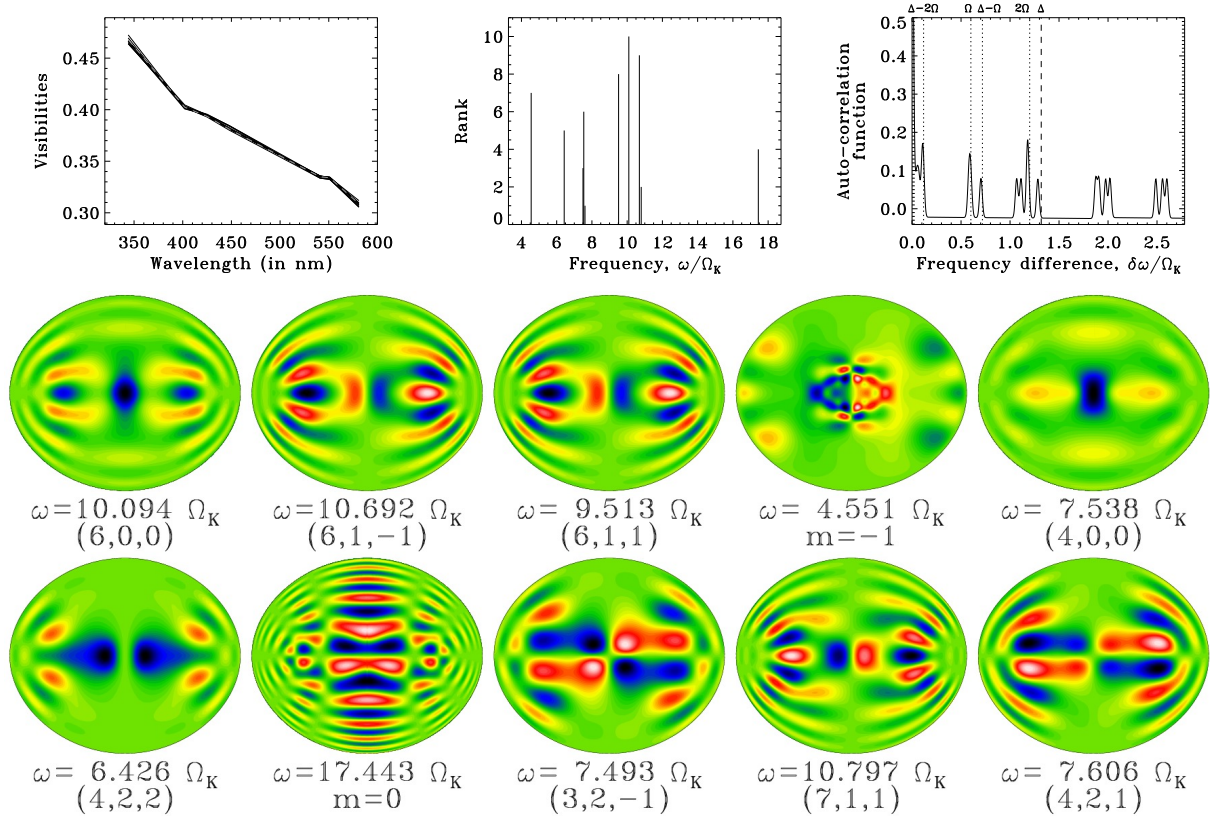


Figure 3.11: A grouping of 10 modes with similar amplitude ratios selected from a large set of modes in a  $2 M_\odot$  SCF model at  $0.6\Omega_K$ . The top row shows, from left to right, the amplitude ratios, the frequency spectrum, and the autocorrelation of the frequency spectrum along with some characteristic frequency spacings. The bottom two rows show the cross section of these modes along with their frequencies and  $(n, \ell, m)$  quantum numbers (taken from Reese et al. 2017b).

depth is neglected. More realistic calculations based on model atmospheres will be needed to come up with more reliable predictions. Tools like FAMIAS (Zima 2008) will then need to be adapted to allow mode identification.

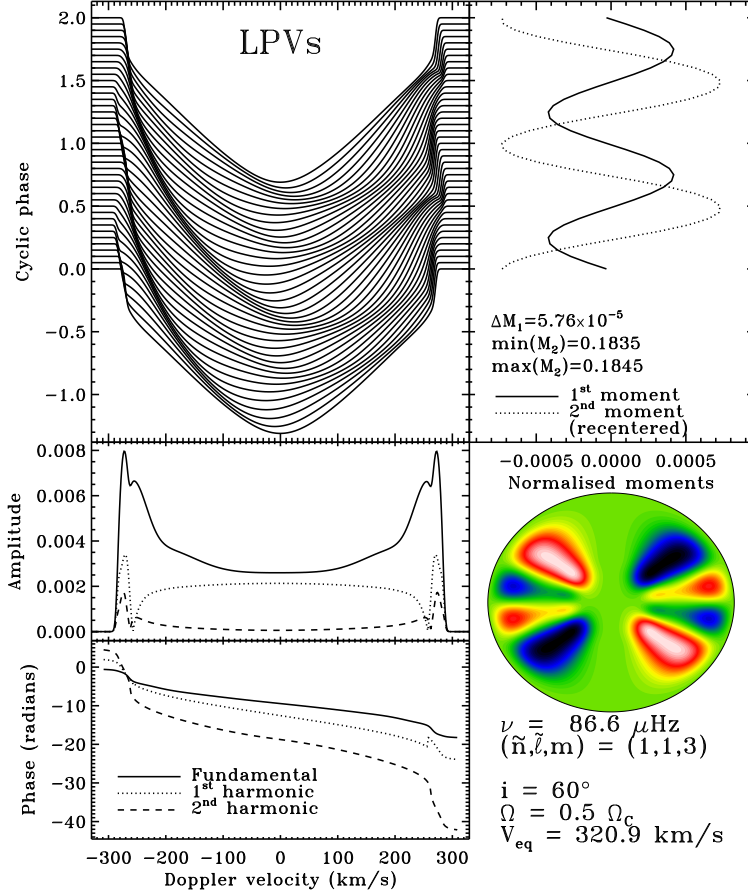


Figure 3.12: Line profile variations in a  $9 M_{\odot}$  ESTER model rotating at  $0.5 \Omega_K$ . The panels from left to right, then top to bottom, are the LPVs, their first and second moments, the amplitudes and phases of the first 3 harmonics of the variations across the line profile, and a cross-section of the pulsation mode (taken from Reese et al. 2017a).

### 3.6 Mode excitation

Non-adiabatic effects are also important for knowing which modes are excited and may potentially be detected in classic pulsators. In some cases, this can help constrain mode identification, particularly in stars with few pulsation modes, such as some  $\beta$  Cep stars. Nonetheless, only two pulsation codes are currently capable of handling non-adiabatic effects in the pulsations of rapidly rotating stars. These are: the code by Lee & Baraffe (1995) and the TOP code (Reese et al. 2017a). Furthermore, only the TOP code uses models from ESTER code, currently the only code which self-consistently solves the energy equation in 2D (Espinosa Lara & Rieutord 2013, Rieutord et al. 2016), a prerequisite for consistent non-adiabatic calculations. Hence, there are relatively few results on the topic, most of them being focused on low frequency modes for which centrifugal deformation is less of an issue (*e.g.* Lee 2013). Accordingly, only a few preliminary results will be presented here.

A first question is what type of modes are excited. Figure 3.13 shows excited modes from several classes, calculated for  $9 M_{\odot}$  stellar models at various rotation rates. Of these,



it seems likely that whispering gallery modes will not be detected due to disc integration effects. A second question is whether there is a preference for prograde or retrograde modes. The left panel of Fig. 3.14 shows the work integral for a mode multiplet. As can be seen, retrograde modes are stabilised first while prograde modes remain excited. This agrees with what Lee (2008) found for gravito-inertial modes. The right panel shows a 2D plot of the work integral using  $\log(T)$  as a radial coordinate. Finally, we note that Mirouh et al. (2017) calculated non-adiabatic pulsation spectra and mode visibilities in an attempt to interpret the seismic observations of Rasalhague ( $\alpha$  Ophiuchi). Although some excited modes are obtained with a semi-regular pattern, more work is needed to obtain fully reliable calculations and in particular reliable mode excitations in that mass range.

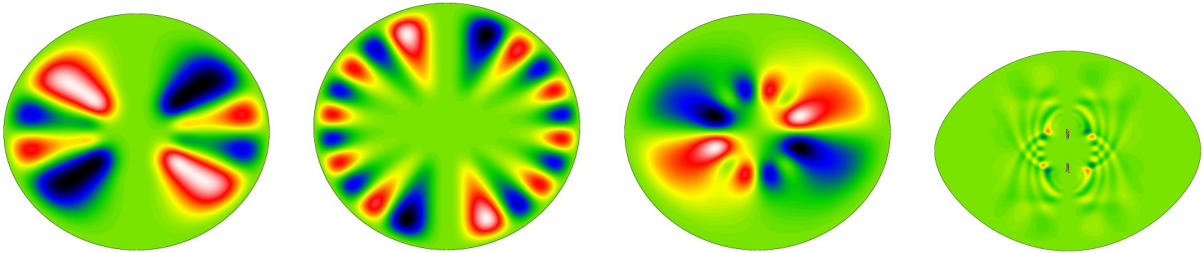


Figure 3.13: Different modes which are excited. These are, from left to right: an island mode, a whispering gallery mode, a mixed mode, and a rosette mode (taken from Reese et al. 2017a).

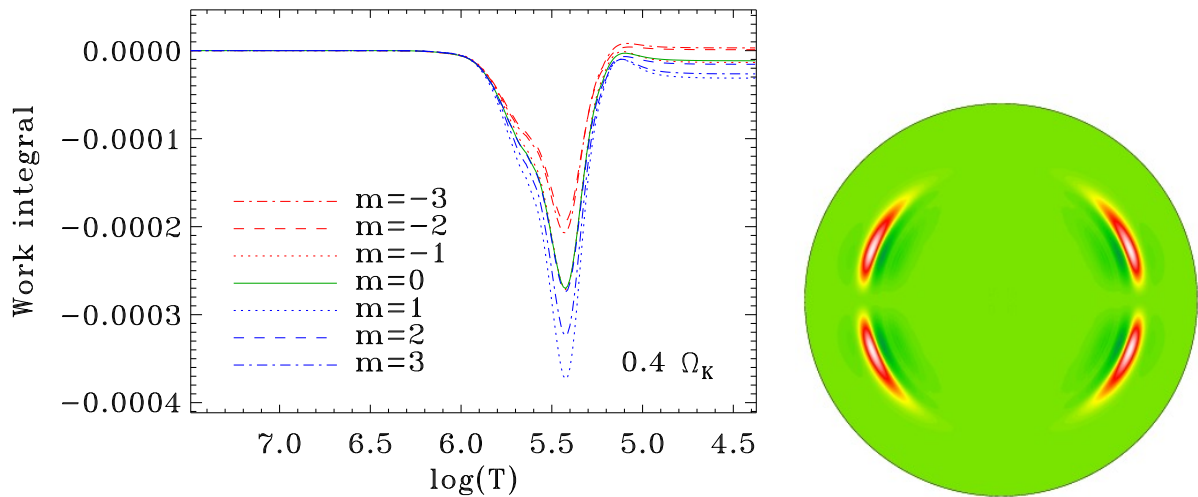


Figure 3.14: (Left) Work integral for a multiplet of modes. The retrograde modes have been stabilised whereas the prograde modes are still excited. (Right) 2D plot of the work integral of the  $m = -2$  mode (which is excited) using  $\log(T)$  as a radial coordinate (with the outer boundary corresponding to the stellar surface) so that the excitation regions (red/white) and damping regions (blue/black) are clearly visible.

# Chapter 4

## Conclusion and perspectives

As can be seen, much progress has been made in the field of asteroseismology thanks to the work of many scientists including the work presented here. For solar-like pulsators, the basic components of what will probably become an asteroseismic pipeline, capable of accurately characterising a large number of stars, are coming together. These include AIMS, a Bayesian code for carrying out forward modelling of observed pulsating stars, InterpolateModel, a code which combines the acoustic structure of multiple models, and InversionPipeline, an inversion tool capable of producing refined estimates of stellar parameters. Another component which I have not worked on but which is equally important is a glitch analysis tool capable of measuring the acoustic depth of the base of the convection zone and various ionisation zones, as well as estimate the amount of helium in the convective envelope. Other components will also be necessary to handle post-main-sequence stars with a few mixed modes that are not in the asymptotic regime (*e.g.* Deheuvels & Michel 2011).

The next steps for this work is to streamline the above tools. For instance, rather than dealing with three different codes, it will be much easier to work with a single program which carries out all of the above steps. In addition the tools need to be made more efficient. For instance, the AIMS code currently takes a few minutes to run with a grid of  $10^5$  models. Increase that to  $10^6$  models and the execution time takes several hours. In addition, storing the grid in memory takes up a large amount of space, which furthermore may be duplicated on each process when AIMS is run in parallel (depending on the exploitation system), probably as a result of AIMS' python implementation. It may therefore be necessary to rewrite parts of the code in a lower level language with a better management of the memory, and only use the parts of the grid relevant to the star being analysed. This would then allow AIMS to handle larger grids, possibly with supplementary dimensions, thus testing a wider range of physical ingredients. In addition to these improvements, it will be necessary to investigate the sources of error at every level of the program, in particular those related to interpolation, and determine how they propagate to the final results. With such a pipeline, it will then be possible to handle the large amount of data expected from future space missions like TESS and PLATO 2.0. It will lead to the production of large homogeneous sets of stellar properties useful not only for stellar physics but also for galactic archaeology and exoplanetary science.

For stars with particularly rich pulsation spectra, in order to extract structural profiles, it will be necessary to put together non-linear iterative inversion tools such as the ones

by Antia & Basu (1994), Antia (1996), Vorontsov et al. (2013), Roxburgh (2015). The `NonLinearKit` tool described in Sect. A.2 is a step in this direction, but a more efficient regularisation is needed in order to obtain well-behaved smooth solutions. Longer term improvements, which could be implemented in collaboration with G. Buldgen, include setting up one or several equations of state in the inversion process. This would then produce physically coherent solutions and may provide ways of testing more detailed aspects of physics. Non-linear inversions may also be useful when inverting rotation profiles in red giants. Indeed, linear inversions frequently produce solutions which are not decreasing throughout the star and which change sign in some cases. Although such solutions may be representative of true physical effects in some cases, they are likely to be a numerical artefact related to the inversion in many cases. Hence, it is necessary to explore the solutions which may be obtained by enforcing supplementary a priori assumptions.

For rapidly rotating pulsators, much progress has been made, particularly in characterising the pulsation spectra of increasingly more realistic rapidly rotating models, implementing non-adiabatic effects in the pulsation calculations, and predicting multicolour amplitude ratios and phase differences, as well as spectroscopic line profile variations. In parallel, progress has been made in interpreting observed pulsation spectra of  $\delta$  Scuti, notably in finding frequency patterns and recurrent spacings (*e.g.* Paparó et al. 2016a,b, Michel et al. 2017) and using them to constrain their mean densities and  $\log(g)$  values (García Hernández et al. 2015, 2017).

Nonetheless, in order to make a real breakthrough in this domain, it is necessary to identify individual modes in the pulsation spectra. So far, this is only starting to be achieved in  $\gamma$  Dor stars and SPBs where clear period spacing patterns in their g-mode pulsation spectra have led to an identification of the azimuthal order and to various seismic diagnostics (*e.g.* Van Reeth et al. 2015, 2016, Ouazzani et al. 2017, 2018, Pápics et al. 2017). For similar progress to be made in the acoustic domain, namely in  $\delta$  Scuti and  $\beta$  Cep stars, several strategies need to be investigated. First of all, a systematic study of the pulsation spectra of a grid of rapidly rotating models needs to be carried out in order to characterise the relationship between model properties and the coefficients in the asymptotic formula for island mode frequencies. Preliminary investigations show that the ratio between some of these coefficients depends primarily on the rotation rate. Using constraints such as these could help guide the search for frequency patterns in observed spectra. If the grid of models is sufficiently large, it may be possible to interpolate the spectra to intermediate points and implement a similar forward modelling approach as what is implemented in AIMS.

However, chaotic modes are also expected to be visible thus complicating the extraction of island mode (Lignières & Georgeot 2009, Reese et al. 2013). This is further compounded by the lack of an adequate non-linear theory capable of predicting mode amplitudes. This brings us to the second strategy, namely applying mode identification techniques. Indeed, amplitude ratios and phase differences from multicolour photometry depend on the geometry and properties of the mode, and not on the intrinsic amplitudes. They can thus be used to constrain the mode identification. Accordingly, it is necessary to systematically calculate amplitude ratios and phase differences using the non-adiabatic version of TOP and models from the ESTER code and compare them with observations. Likewise, line profile variations also provide constraints on mode geometry and identification, constraints which are often complementary to those from multicolour photometry.

Hence a systematic survey of theoretical line profile variations needs to be carried out and implemented in a tool like FAMIAS (Zima 2008) in order to carry out mode identification. Intermediate results used to calculate amplitude ratios, phases differences, and line profile variations need to be stored in a database from which future mode identification tools could operate.

In addition, mode excitation mechanisms need to be studied in a systematic way using the non-adiabatic version of TOP. This would then help with the interpretation of stars with relatively few detected pulsation modes, for instance by ruling out potential identifications if the relevant modes are not excited in the model. Combining all of these strategies should hopefully lead to a clear identification of modes in rapidly rotating acoustic pulsators. This would then help with obtaining precise stellar properties, and in some cases with constraining the internal structure of these stars. For instance, it may be possible to probe differential rotation using the rotation kernels described in Sect. 3.4.1 and inversion methods. Achieving success in this domain would open up new regions of the HR diagram to asteroseismology and would enable us to test stellar physics in parameter regimes that have so far not been accessible.

Longer term, it will be interesting to include supplementary ingredients such as magnetic fields and tidal deformation in the TOP pulsation code. This would imply extending the code's capability to 3D problems which of course would require much more numerical resources. As a preliminary step in this direction, the code has partially been parallelised using appropriate numerical libraries for distributed memory supercomputers. Once the code is functioning correctly, it would then allow us to study roAp stars (*e.g.* Kurtz 1990), other magnetic rotating pulsating stars, including neutron stars, and pulsating stars in close binary systems, thus bringing new physical insights into these objects.

Beyond the progress in stellar physics, some of the results described above may also be applied to rapidly rotating planets such as Jupiter and Saturn, at 30% and 40% of the critical rotation rate, respectively. Indeed, the goal of the JOVIAL project is to observe pulsation modes in Jupiter (Schmider et al. 2013). Already, a large frequency separation, comparable to that of the sun has been observed (Gaulme et al. 2011). Given the proximity of Jupiter, it may be possible to obtain resolved images of the pulsations thus considerably facilitating the identification of modes. TOP could then calculate pulsation modes in Jovian models, which in turn could be used to probe its internal structure and answer key questions such as whether Jupiter has a solid core. Preliminary collaborations have already allowed me to provide an accurate and rapid method for calculating gravitational moments of a given centrifugally-deformed model which have subsequently been compared with Juno observations (Wahl et al. 2017, Guillot et al. 2018) and to put together a simple and rapid code for deforming a 1D model thanks to the centrifugal force (see Sect. A.5.1).



# Chapter 5

## Bibliography

- Aerts, C., Christensen-Dalsgaard, J., & Kurtz, D. W. 2010, *Asteroseismology*, Astronomy and Astrophysics Library (Springer-Verlag)
- Antia, H. M. 1996, *A&A*, 307, 609
- Antia, H. M. & Basu, S. 1994, *A&A Supp.*, 107, 421
- Auriac, J. 2011, Master's thesis, ENSPS, under the supervision of J. J. Green and R. Samadi
- Aurière, M. 2003, in *EAS Publications Series*, Vol. 9, *EAS Publications Series*, ed. J. Arnaud & N. Meunier, 105
- Auvergne, M., Bodin, P., Boissard, L., et al. 2009, *A&A*, 506, 411
- Baglin, A., Auvergne, M., Barge, P., et al. 2009, in *IAU Symposium*, Vol. 253, *IAU Symposium*, 71–81
- Ballot, J., Lignières, F., Prat, V., Reese, D. R., & Rieutord, M. 2012, in *Astronomical Society of the Pacific Conference Series*, Vol. 462, *Progress in Solar/Stellar Physics with Helio- and Asteroseismology*, ed. H. Shibahashi, M. Takata, & A. E. Lynas-Gray, 389
- Ballot, J., Lignières, F., & Reese, D. R. 2013, in *Lecture Notes in Physics*, Vol. 865, *Lecture Notes in Physics*, ed. M. Goupil, K. Belkacem, C. Neiner, F. Lignières, & J. J. Green (Berlin Springer Verlag), 91
- Ballot, J., Lignières, F., Reese, D. R., & Rieutord, M. 2010, *A&A*, 518, A30
- Basu, S., Christensen-Dalsgaard, J., Chaplin, W. J., et al. 1997, *MNRAS*, 292, 243
- Bazot, M., Bourguignon, S., & Christensen-Dalsgaard, J. 2012, *MNRAS*, 427, 1847
- Beck, P. G., Montalbán, J., Kallinger, T., et al. 2012, *Nature*, 481, 55
- Berthomieu, G., Gónczi, G., Graff, P., Provost, J., & Rocca, A. 1978, *A&A*, 70, 597
- Borucki, W., Koch, D., Batalha, N., et al. 2009, in *IAU Symposium*, Vol. 253, *IAU Symposium*, 289–299
- Bouabid, M.-P., Dupret, M.-A., Salmon, S., et al. 2013, *MNRAS*, 429, 2500
- Brassard, P., Fontaine, G., Billères, M., et al. 2001, *ApJ*, 563, 1013
- Brott, I., Evans, C. J., Hunter, I., et al. 2011, *A&A*, 530, A116
- Buldgen, G., Reese, D., & Dupret, M.-A. 2017a, in *European Physical Journal Web of Conferences*, Vol. 160, *European Physical Journal Web of Conferences*, 03005
- Buldgen, G., Reese, D. R., & Dupret, M. A. 2015a, *A&A*, 583, A62
- 2016a, *A&A*, 585, A109
- 2017b, *A&A*, 598, A21
- 2018, *A&A*, 609, A95
- Buldgen, G., Reese, D. R., Dupret, M. A., & Samadi, R. 2015b, *A&A*, 574, A42
- Buldgen, G., Salmon, S. J. A. J., Godart, M., et al. 2017c, *MNRAS*, 472, L70
- Buldgen, G., Salmon, S. J. A. J., Noels, A., et al. 2017d, *MNRAS*, 472, 751
- 2017e, *A&A*, 607, A58

- Buldgen, G., Salmon, S. J. A. J., Reese, D. R., & Dupret, M. A. 2016b, *A&A*, 596, A73
- Burke, K. D., Reese, D. R., & Thompson, M. J. 2011, *MNRAS*, 414, 1119
- Casagrande, L., Silva Aguirre, V., Stello, D., et al. 2014, *ApJ*, 787, 110
- Catala, C., Appourchaux, T., & Plato Mission Consortium. 2011, *Journal of Physics Conference Series*, 271, 012084
- Ceillier, T., Eggenberger, P., García, R. A., & Mathis, S. 2013, *A&A*, 555, A54
- Chaplin, W. J., Basu, S., Huber, D., et al. 2014, *ApJS*, 210, 1
- Charpinet, S., Fontaine, G., Brassard, P., Green, E. M., & Chayer, P. 2005, *A&A*, 437, 575
- Christensen-Dalsgaard, J. 2008, *ApSS*, 316, 13
- . 2014, *Asteroseismology of red giants*, ed. P. L. Pallé & C. Esteban, 194
- Christensen-Dalsgaard, J., Gough, D. O., & Morgan, J. G. 1979, *A&A*, 73, 121
- Christensen-Dalsgaard, J., Schou, J., & Thompson, M. J. 1990, *MNRAS*, 242, 353
- Clement, M. J. 1994, in *IAU Symp. 162: Pulsation; Rotation; and Mass Loss in Early-Type Stars*, ed. L. A. Balona, H. F. Henrichs, & J. M. Le Contel, 117
- Coelho, H. R., Chaplin, W. J., Basu, S., et al. 2015, *MNRAS*, 451, 3011
- Daszyńska-Daszkiewicz, J., Dziembowski, W. A., Jerzykiewicz, M., & Handler, G. 2015, *MNRAS*, 446, 1438
- Daszynska-Daszkiewicz, J., Dziembowski, W. A., & Pamyatnykh, A. A. 2007, *Acta Astronomica*, 57, 11
- Daszyńska-Daszkiewicz, J., Dziembowski, W. A., Pamyatnykh, A. A., & Goupil, M.-J. 2002, *A&A*, 392, 151
- Deeg, H. & Belmonte, J. 2018, *Handbook of Exoplanets*, *Handbook of Exoplanets* (Springer International Publishing)
- Deheuvels, S., Doğan, G., Goupil, M. J., et al. 2014, *A&A*, 564, A27
- Deheuvels, S., García, R. A., Chaplin, W. J., et al. 2012, *ApJ*, 756, 19
- Deheuvels, S. & Michel, E. 2011, *A&A*, 535, A91
- Deupree, R. G. 2011, *ApJ*, 742, 9
- Dintrans, B. & Rieutord, M. 2000, *A&A*, 354, 86
- Domiciano de Souza, A., Kervella, P., Jankov, S., et al. 2003, *A&A*, 407, L47
- Donati, J.-F. 2003, in *Astronomical Society of the Pacific Conference Series*, Vol. 307, *Solar Polarization*, ed. J. Trujillo-Bueno & J. Sanchez Almeida, 41
- Donati, J.-F., Howarth, I. D., Jardine, M. M., et al. 2006, *MNRAS*, 370, 629
- Dupret, M.-A., De Ridder, J., De Cat, P., et al. 2003, *A&A*, 398, 677
- Dupret, M.-A., Grigahcène, A., Garrido, R., Gabriel, M., & Scuflaire, R. 2004, *A&A*, 414, L17
- Dziembowski, W., Krolikowska, M., & Kosovichev, A. 1988, *Acta Astronomica*, 38
- Eggenberger, P., Meynet, G., Maeder, A., et al. 2008, *ApSS*, 316, 43
- Eggenberger, P., Montalbán, J., & Miglio, A. 2012, *A&A*, 544, L4
- Ekström, S., Meynet, G., Chiappini, C., Hirschi, R., & Maeder, A. 2008, *A&A*, 489, 685
- Espinosa Lara, F. & Rieutord, M. 2013, *A&A*, 552, A35
- Foreman-Mackey, D., Hogg, D. W., Lang, D., & Goodman, J. 2013, *PASP*, 125, 306
- García Hernández, A., Martín-Ruiz, S., Monteiro, M. J. P. F. G., et al. 2015, *ApJL*, 811, L29
- García Hernández, A., Moya, A., Michel, E., et al. 2009, *A&A*, 506, 79
- . 2013, *A&A*, 559, A63
- García Hernández, A., Suárez, J. C., Moya, A., et al. 2017, *MNRAS*, 471, L140
- Gaulme, P., Schmider, F.-X., Gay, J., Guillot, T., & Jacob, C. 2011, *A&A*, 531, A104
- Gough, D. 1985, *Sol. Phys.*, 100, 65
- Gough, D. O. & Thompson, M. J. 1991, *The inversion problem*, ed. Cox, A. N., Livingston, W. C., & Matthews, M. S. (University of Arizona Press, Tucson), 519–561
- Goupil, M.-J., Dupret, M. A., Samadi, R., et al. 2005, *JA&A*, 26, 249

- Green, J. J. 2010a, Feasibility of the voxel PSF representation, Tech. Rep. PLATO-GS-TN-240-LESIA, LESIA, Observatoire de Paris
- . 2010b, Voxel representation for the PLATO point spread function, Tech. Rep. PLATO-GS-TN-239-LESIA, LESIA, Observatoire de Paris
- . 2011a, Microscanning, Tech. Rep. PLATO-GS-TN-231-LESIA, LESIA, Observatoire de Paris
- . 2011b, PSF inversion with the Landweber iteration, Tech. Rep. PLATO-GS-TN-230-LESIA, LESIA, Observatoire de Paris
- Grundahl, F., Arentoft, T., Christensen-Dalsgaard, J., et al. 2008, in *Journal of Physics Conference Series*, Vol. 118, *Journal of Physics Conference Series*, 012041
- Guillot, T. & Havel, M. 2011, *A&A*, 527, A20
- Guillot, T., Miguel, Y., Militzer, B., et al. 2018, *Nature*, 555, 227
- Guillot, T. & Morel, P. 1995, *A&A Supp.*, 109, 109
- Heger, A. & Langer, N. 2000, *ApJ*, 544, 1016
- Hunter, I., Brott, I., Lennon, D. J., et al. 2008, *ApJ*, 676, L29
- Jackson, S., MacGregor, K. B., & Skumanich, A. 2004, *ApJ*, 606, 1196
- . 2005, *ApJS*, 156, 245
- Kervella, P. 2016, in *Lecture Notes in Physics*, Berlin Springer Verlag, Vol. 914, *Lecture Notes in Physics*, Berlin Springer Verlag, ed. J.-P. Rozelot & C. Neiner, 127
- Kervella, P. & Domiciano de Souza, A. 2006, *A&A*, 453, 1059
- Kjeldsen, H., Bedding, T. R., & Christensen-Dalsgaard, J. 2008, *ApJ*, 683, L175
- Kurtz, D. W. 1990, *ARA&A*, 28, 607
- Kuschnig, R., Weiss, W. W., Moffat, A., & Kudelka, O. 2009, in *Astronomical Society of the Pacific Conference Series*, Vol. 416, *Solar-Stellar Dynamos as Revealed by Helio- and Asteroseismology: GONG 2008/SOHO 21*, ed. M. Dikpati, T. Arentoft, I. González Hernández, C. Lindsey, & F. Hill, 587
- Ledoux, P. 1951, *ApJ*, 114, 373
- Lee, U. 2006, *MNRAS*, 365, 677
- Lee, U. 2008, in *American Institute of Physics Conference Series*, Vol. 1043, *American Institute of Physics Conference Series*, ed. V. Mioc, C. Dumitrche, & N. A. Popescu, 344–350
- Lee, U. 2013, in *Lecture Notes in Physics*, Berlin Springer Verlag, Vol. 865, *Lecture Notes in Physics*, Berlin Springer Verlag, ed. M. Goupil, K. Belkacem, C. Neiner, F. Lignières, & J. J. Green, 133
- Lee, U. & Baraffe, I. 1995, *A&A*, 301, 419
- Lee, U. & Saio, H. 1987, *MNRAS*, 224, 513
- Lignières, F. & Georgeot, B. 2008, *Phys. Rev. E*, 78, 016215
- . 2009, *A&A*, 500, 1173
- Lignières, F., Georgeot, B., & Ballot, J. 2010, *Astronomische Nachrichten*, 331, 1053
- Lignières, F., Rieutord, M., & Reese, D. 2006, *A&A*, 455, 607
- Lynden-Bell, D. & Ostriker, J. P. 1967, *MNRAS*, 136, 293
- MacGregor, K. B., Jackson, S., Skumanich, A., & Metcalfe, T. S. 2007, *ApJ*, 663, 560
- Maeder, A. 2009, *Physics, Formation and Evolution of Rotating Stars*, *Astronomy and Astrophysics Library* (Springer-Verlag)
- Maeder, A. & Meynet, G. 2001, *A&A*, 373, 555
- Mantegazza, L., Poretti, E., Michel, E., et al. 2012, *A&A*, 542, A24
- Marques, J. P., Goupil, M. J., Lebreton, Y., et al. 2013, *A&A*, 549, A74
- Martins, F., Simón-Díaz, S., Barbá, R. H., Gamen, R. C., & Ekström, S. 2017, *A&A*, 599, A30
- Matthews, J. M., Kuschnig, R., Guenther, D. B., et al. 2004, *Nature*, 430, 51
- Metcalfe, T. S., Creevey, O. L., & Christensen-Dalsgaard, J. 2009, *ApJ*, 699, 373
- Metcalfe, T. S., Creevey, O. L., Doğan, G., et al. 2014, *ApJS*, 214, 27



- Metcalfe, T. S., Monteiro, M. J. P. F. G., Thompson, M. J., et al. 2010, *ApJ*, 723, 1583
- Meynet, G. & Maeder, A. 2000, *A&A*, 361, 101
- . 2003, *A&A*, 404, 975
- Meynet, G. & Maeder, A. 2005a, in *Astronomical Society of the Pacific Conference Series*, Vol. 337, *The Nature and Evolution of Disks Around Hot Stars*, ed. R. Ignace & K. G. Gayley, 15
- . 2005b, *A&A*, 429, 581
- Michel, E., Dupret, M.-A., Reese, D., et al. 2017, in *European Physical Journal Web of Conferences*, Vol. 160, *European Physical Journal Web of Conferences*, 03001
- Miglio, A., Chiappini, C., Morel, T., et al. 2013, *MNRAS*, 429, 423
- Mirouh, G. M., Reese, D. R., Lara, F. E., Ballot, J., & Rieutord, M. 2014, in *IAU Symposium*, Vol. 301, *Precision Asteroseismology*, ed. J. A. Guzik, W. J. Chaplin, G. Handler, & A. Pigulski, 455–456
- Mirouh, G. M., Reese, D. R., Rieutord, M., & Ballot, J. 2017, in *SF2A-2017: Proceedings of the Annual meeting of the French Society of Astronomy and Astrophysics*, ed. C. Reylé, P. Di Matteo, F. Herpin, E. Lagadec, A. Lançon, Z. Meliani, & F. Royer, 103–106
- Monnier, J. D., Zhao, M., Pedretti, E., et al. 2007, *Science*, 317, 342
- Mosser, B., Goupil, M. J., Belkacem, K., et al. 2012, *A&A*, 540, A143
- Nsamba, B., Campante, T. L., Monteiro, M. J. P. F. G., et al. 2018, *MNRAS*, in press
- Ouazzani, R.-M., Dupret, M.-A., & Reese, D. R. 2012, *A&A*, 547, A75
- Ouazzani, R.-M., Green, J., & Samadi, R. 2015a, *Modeling PLATO PSF using microscanning technique: study of different scenarios and requirements*, Tech. Rep. PLATO-LESIA-PDC-TN-013, LESIA, Observatoire de Paris
- Ouazzani, R.-M., Marques, J. P., Goupil, M., et al. 2018, *A&A*, submitted, astro-ph.SR/1801.09228
- Ouazzani, R.-M., Roxburgh, I. W., & Dupret, M.-A. 2015b, *A&A*, 579, A116
- Ouazzani, R.-M., Salmon, S. J. A. J., Antoci, V., et al. 2017, *MNRAS*, 465, 2294
- Palacios, A., Talon, S., Charbonnel, C., & Forestini, M. 2003, *A&A*, 399, 603
- Papaloizou, J. & Pringle, J. E. 1978, *MNRAS*, 182, 423
- Papará, M., Benkó, J. M., Hareter, M., & Guzik, J. A. 2016a, *ApJ*, 822, 100
- . 2016b, *ApJS*, 224, 41
- Pápics, P. I., Tkachenko, A., Van Reeth, T., et al. 2017, *A&A*, 598, A74
- Pasek, M., Georgeot, B., Lignières, F., & Reese, D. R. 2011, *Physical Review Letters*, 107, 121101
- Pasek, M., Lignières, F., Georgeot, B., & Reese, D. R. 2012, *A&A*, 546, A11
- Perryman, M. A. C., de Boer, K. S., Gilmore, G., et al. 2001, *A&A*, 369, 339
- Peterson, D. M., Hummel, C. A., Pauls, T. A., et al. 2006, *ApJ*, 636, 1087
- Pijpers, F. P. & Thompson, M. J. 1992, *A&A*, 262, L33
- . 1994, *A&A*, 281, 231
- Piskunov, N., Snik, F., Dolgoplov, A., et al. 2011, *The Messenger*, 143, 7
- Poretti, E., Michel, E., Garrido, R., et al. 2009, *A&A*, 506, 85
- Prantzos, N. & Boissier, S. 2003, *A&A*, 406, 259
- Prat, V., Mathis, S., Augustson, K., et al. 2018, *A&A*, in press, astro-ph.SR/1803.04229
- Rauer, H., Catala, C., Aerts, C., et al. 2014, *Experimental Astronomy*, 38, 249
- Reese, D., Lignières, F., & Rieutord, M. 2006, *A&A*, 455, 621
- . 2008, *A&A*, 481, 449
- Reese, D. R. 2013, *A&A*, 555, A148
- . 2015, *A&A*, 578, A37
- Reese, D. R., Chaplin, W. J., Davies, G. R., et al. 2016, *A&A*, 592, A14
- Reese, D. R., Dupret, M.-A., & Rieutord, M. 2017a, in *European Physical Journal Web of*

- Conferences, Vol. 160, European Physical Journal Web of Conferences, 02007
- Reese, D. R., Dupret, M.-A., & Rieutord, M. 2018, in 3rd BRITE Science Workshop, in press, astro-ph.SR/1803.07442
- Reese, D. R., Espinosa Lara, F., & Rieutord, M. 2011, in IAU Symposium, Vol. 272, Active OB Stars: Structure, Evolution, Mass Loss, and Critical Limits, ed. C. Neiner, G. Wade, G. Meynet, & G. Peters, 535–536
- Reese, D. R., Lara, F. E., & Rieutord, M. 2014, in IAU Symposium, Vol. 301, Precision Asteroseismology, ed. J. A. Guzik, W. J. Chaplin, G. Handler, & A. Pigulski, 169–172
- Reese, D. R., Lignières, F., Ballot, J., et al. 2017b, *A&A*, 601, A130
- Reese, D. R., MacGregor, K. B., Jackson, S., Skumanich, A., & Metcalfe, T. S. 2009a, *A&A*, 506, 189
- Reese, D. R., Marques, J. P., Goupil, M. J., Thompson, M. J., & Deheuvels, S. 2012, *A&A*, 539, A63
- Reese, D. R., Prat, V., Barban, C., van 't Veer-Menneret, C., & MacGregor, K. B. 2013, *A&A*, 550, A77
- Reese, D. R., Thompson, M. J., MacGregor, K. B., et al. 2009b, *A&A*, 506, 183
- Reese, D. R. 2016, 1D and 2D PSF interpolation schemes based on triangulation and associated tests, Tech. Rep. PLATO-LESIA-PDC-TN-024\_i1.3, LESIA, Observatoire de Paris
- . 2017a, A comparison between the MART and Positive RLS inversion methods, Tech. Rep. PLATO-LESIA-PDC-TN-032\_i1.1, LESIA, Observatoire de Paris
- . 2017b, An alternate algorithm for Positive RLS inversions, Tech. Rep. PLATO-LESIA-PDC-TN-0035\_i1.1, LESIA, Observatoire de Paris
- . 2017c, The weighted Positive RLS inversion method, Tech. Rep. PLATO-LESIA-PDC-TN-0037\_i1.0, LESIA, Observatoire de Paris
- Ricker, G. R., Winn, J. N., VanderSpek, R., et al. 2015, *Journal of Astronomical Telescopes, Instruments, and Systems*, 1, 014003
- Rieutord, M. & Espinosa Lara, F. 2013, in *Lecture Notes in Physics*, Berlin Springer Verlag, Vol. 865, *Lecture Notes in Physics*, Berlin Springer Verlag, ed. M. Goupil, K. Belkacem, C. Neiner, F. Lignières, & J. J. Green, 49
- Rieutord, M., Espinosa Lara, F., & Putigny, B. 2016, *Journal of Computational Physics*, 318, 277
- Rieutord, M., Georgeot, B., & Valdetaro, L. 2001, *Journal of Fluid Mechanics*, 435, 103
- Roxburgh, I. W. 2015, *A&A*, 574, A45
- . 2016, *A&A*, 585, A63
- Royer, F. 2009, in *Lecture Notes in Physics*, Berlin Springer Verlag, Vol. 765, *The Rotation of Sun and Stars*, 207–230
- Saio, H. & Takata, M. 2014, *Publications of the Astronomical Society of Japan*, 66, 58
- Savonije, G. J. 2013, *A&A*, 559, A25
- Schmider, F. X., Appourchaux, T., Gaulme, P., et al. 2013, in *Astronomical Society of the Pacific Conference Series*, Vol. 478, *Fifty Years of Seismology of the Sun and Stars*, ed. K. Jain, S. C. Tripathy, F. Hill, J. W. Leibacher, & A. A. Pevtsov, 119
- Schou, J., Antia, H. M., Basu, S., et al. 1998, *ApJ*, 505, 390
- Semel, M. 1989, *A&A*, 225, 456
- Serenelli, A. M., Bergemann, M., Ruchti, G., & Casagrande, L. 2013, *MNRAS*, 429, 3645
- Silva Aguirre, V., Davies, G. R., Basu, S., et al. 2015, *MNRAS*, 452, 2127
- Silva Aguirre, V., Lund, M. N., Antia, H. M., et al. 2017, *ApJ*, 835, 173
- Suárez, J. C., García Hernández, A., Moya, A., et al. 2014, *A&A*, 563, A7
- Takata, M. & Saio, H. 2013, *Publications of the Astronomical Society of Japan*, 65, 68
- Tassoul, M. 1980, *ApJS*, 43, 469

- Thompson, M. J., Christensen-Dalsgaard, J., Miesch, M. S., & Toomre, J. 2003, *ARA&A*, 41, 599
- Townsend, R. H. D. 1997, *MNRAS*, 284, 839
- 2003a, *MNRAS*, 343, 125
- 2003b, *MNRAS*, 340, 1020
- Van Grootel, V., Charpinet, S., Brassard, P., Fontaine, G., & Green, E. M. 2013, *A&A*, 553, A97
- Van Reeth, T., Tkachenko, A., & Aerts, C. 2016, *A&A*, 593, A120
- Van Reeth, T., Tkachenko, A., Aerts, C., et al. 2015, *ApJS*, 218, 27
- Vorontsov, S. V., Baturin, V. A., Ayukov, S. V., & Gryaznov, V. K. 2013, *MNRAS*, 430, 1636
- Wahl, S. M., Hubbard, W. B., Militzer, B., et al. 2017, *Geoph. Res. Letters*, 44, 4649
- Walker, G., Matthews, J., Kuschnig, R., et al. 2003, *PASP*, 115, 1023
- Woosley, S. E. & Heger, A. 2006, *ApJ*, 637, 914
- Zahn, J.-P. 1992, *A&A*, 265, 115
- Zhao, M., Monnier, J. D., Pedretti, E., et al. 2009, *ApJ*, 701, 209
- Zima, W. 2008, *Communications in Asteroseismology*, 157, 387
- Zinnecker, H. & Yorke, H. W. 2007, *ARA&A*, 45, 481

# Appendix A

## Complementary note

In this chapter, I will describe the various duties I have carried out over the years in addition to my research, including teaching and supervision of Master’s and PhD students. Indeed, during my postdocs in Sheffield (2006-2009) and Birmingham (2014-2015), I worked for scientific networks funded by the European Union, and as such, produced a number of deliverables as well as helped with organising various activities. These will be described in Sects. A.1 and A.2, respectively. Since becoming an associate astronomer at the Observatoire de Paris at Meudon, I carry out an astronomer’s duty (“*tâche de service*” in French) as part of that position (see Sect. A.3). During my Sheffield and Birmingham postdocs, and within the context of my current position, I have carried out various teaching duties (see Sect. A.4). Finally, I have had the opportunity to supervise the internship of 2 Master’s student, co-supervise a PhD student and am currently co-supervising another PhD student as will be described in Sect. A.5.

### A.1 Work for the HELAS network

The European HELio- and ASteroseismology Network (HELAS) was funded as a Coordination Action under the European Union’s Sixth Framework Programme. As such it helped structure and coordinate helio- and asteroseismology research activities within the European community and beyond. From 2006 to 2009, I carried out my Sheffield postdoc working for the Global Helioseismology branch of the HELAS network. This included producing software, helping with the organisation of workshops, and setting up a website for this branch with various articles, documentation, software, and links.

The software developed for the HELAS network are as follows:

- **InversionKit**: software for carrying out inversions of stellar rotation and structural profiles, and later on, the mean density (as based on Reese et al. 2012)
- **Splittings**: software for calculating rotational splittings for 2D rotation profiles (see Fig. A.1 for a screen capture of this program)
- **Echelle**: utility for visualising echelle diagrams
- **SurfCorrect**: utility for applying the surface correction from Kjeldsen et al. (2008, ApJL 683, 175)
- **ReadAMDL**: utility for reading and visualising stellar models in the AMDL and FAMDL formats, compatible with the ADIPLS pulsation code

- **ReadFAMDE**: utility for reading and visualising pulsation modes in the AMDE and FAMDE formats from the ADIPLS pulsation code

All of these programs were written in Java so that they could be run in a web-browser<sup>1</sup> or as a stand-alone application. They are highly interactive and well documented, thus allowing a simple usage of the programs by non-specialists. The **InversionKit** program was extensively used and adapted by G. Buldgen during his PhD (see Sect. A.5).

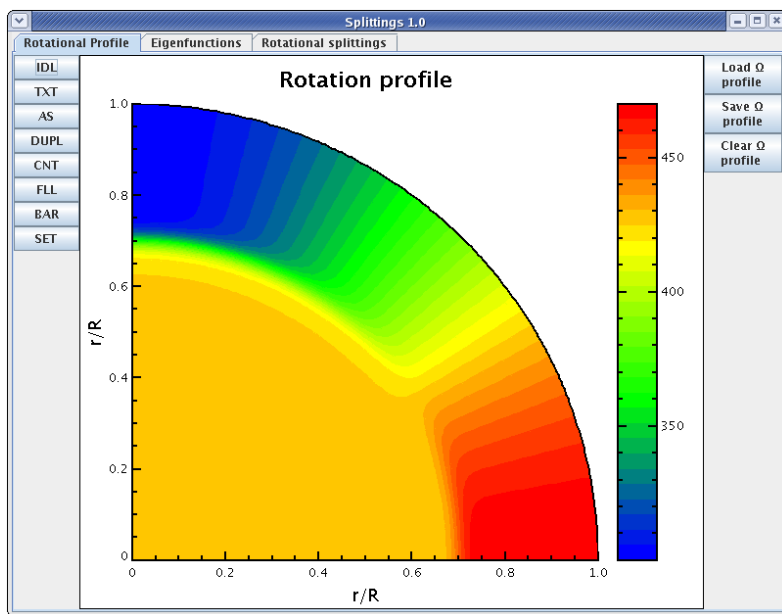


Figure A.1: Screen-capture of the Splittings program, written for the HELAS network.

I participated in the organisation of the “Low degree and low frequency modes” HELAS workshop at La Palma in 2007 and to a lesser degree in that of the “The Acoustic Solar Cycle” HELAS workshop in Birmingham in 2009. This included helping with setting up the program (and putting it on the website), contacting various speakers, and helping with editing the proceedings. Finally, I translated CESAM2k’s quick reference from French into English (about 60 pages worth of translation) and made this available on the HELAS Global Helioseismology website<sup>2</sup>. This, of course, facilitates the use of CESAM2k by non-French speakers.

## A.2 Work for the SpaceInn network

The “Exploitation of Space Data for Innovative Helio- and Asteroseismology” network (SpaceInn) was funded as a collaborative Project under the European Union’s Seventh Framework Programme. The goal of this network is to make full use of space data as well as complementary ground observations in order to gain a better understanding of solar and stellar interiors. It relies on establishing coordinated, long-term data archives which include derived products and analysis tools, coordinating the use of these data, and

<sup>1</sup>Unfortunately, due to security issues, most browsers today do not allow Java applets to run within them.

<sup>2</sup>This documentation is currently available at the following address: [https://www.helas-project.eu/wp-content/uploads/Software/global/models/CESAM\\_quick\\_reference.pdf](https://www.helas-project.eu/wp-content/uploads/Software/global/models/CESAM_quick_reference.pdf)

increasing the public awareness of this field. From 2014 to 2015, I carried out my Birmingham postdoc working for the Asteroseismology branch of the network. This involved producing scientific software, carrying out a hare-and-hounds exercise in order to compare and validate different methods for interpreting a combination of seismic and classic stellar data, and writing relevant articles.

The software developed for the SpaceInn network are as follows:

- **AIMS** (Asteroseismic Inference on a Massive Scale): Python code which estimates stellar parameters from classical and seismic data using an MCMC method
- **InversionKit**: interactive Java code for carrying out inversions of stellar rotation profiles, structure, and integrated quantities (see Fig. A.2).
- **InversionPipeline**: interactive Java code for carrying out inversions of integrated quantities from a grid of models
- **InterpolateModel**: interactive Java code which allows the user to combine the acoustic structure of multiple stellar models
- **NonLinearKit**: experimental interactive Java code for carrying out non-linear seismic structural inversions in stars

The **InversionKit** code was considerably enhanced during my Birmingham postdoc. Supplementary features include: an integrated pulsation code which can deal with discontinuities in the model, enhanced model treatment (accepts more model formats, can manipulate the models in various ways, provides detailed information at each grid point), possibility of inverting supplementary profiles and integrated quantities (the latter being provided by G. Buldgen during his PhD – see Sect. A.5), self-consistency tests on rotational splittings (see Reese 2015), an integrated echelle diagram, and the possibility of adjusting fundamental constants such as the gravitational constant. Figure A.2 provides a screen-capture of the program.

A detailed description of the AIMS code and its scientific and technical aspects is provided in Sect. 2.2. Here, we will look at some of the other aspects of this code. **AIMS** was written in Python in order to facilitate additional contributions from others in the field. This has allowed B. Rendle, a PhD student in Birmingham, to extend it use to red-giants. Furthermore, students at the “Asteroseismology and Exoplanets: Listening to the Stars and Searching for New Worlds” summer school were taught how to use this code. Likewise, the “Stellar Parameters INferred Systematically” (**SPInS**<sup>3</sup>), a spin-off of the AIMS code in which the seismic part has been removed, was used for one of the hands-on sessions at the “5<sup>th</sup> International Young Astronomers School: Scientific Exploitation of the Gaia Data”. Both of these codes may become reference codes or provide ideas for exploiting PLATO 2.0 and Gaia data.

The **AIMS**, **InterpolateModel**, and **InversionPipeline** codes were designed to work together. Typically, **AIMS** produces a sample of representative models, or more precisely a set of coefficients from which to interpolate models, for a set of classic and seismic constraints. **InterpolateModel** can then use these coefficients to interpolate<sup>4</sup> the acoustic

<sup>3</sup>The name of this code is likely to change in the near future.

<sup>4</sup>Here, the word “interpolate” refers to interpolating between multiple models, rather than interpolating a given model to a finer mesh.

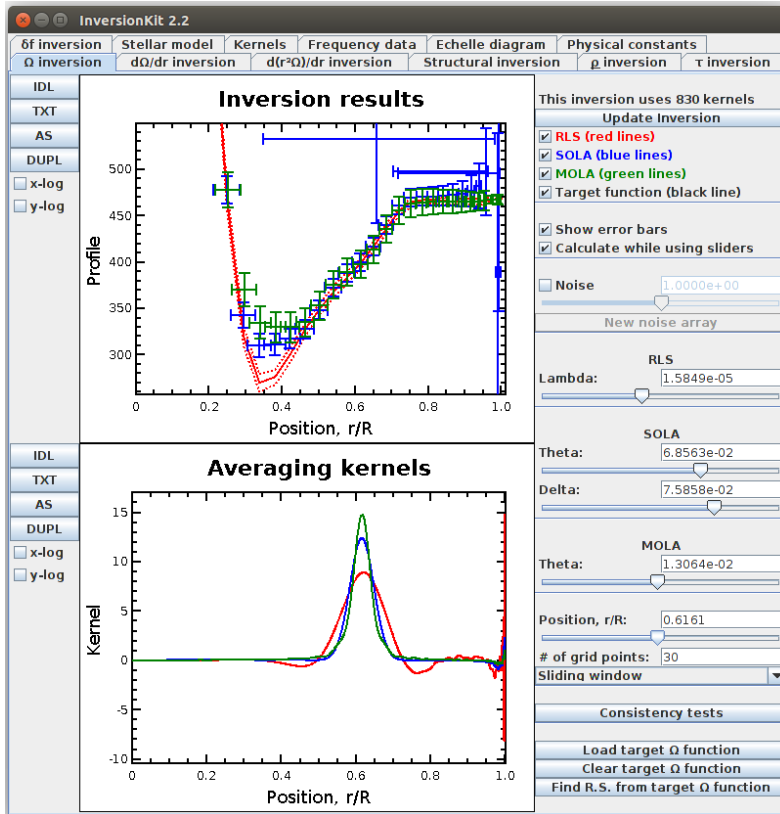


Figure A.2: Screen-capture of the InversionKit program, initially written for the HELAS network and improved for the SpaceInn network.

structure of these modes. Finally, `InversionPipeline` can systematically apply inversions of integrated quantities to these interpolated models in order to obtain a refined estimate of these quantities. The left panel of Fig. A.3 illustrates the sound profiles of interpolated models representative of KIC 10963065 obtained via `InterpolateModel` and the right panel shows the corresponding inverted mean densities, obtained with `InversionPipeline`.

The hare-and-hounds exercise carried out for SpaceInn involved producing a number of models from which to calculate “observed” pulsation spectra and classic constraints. These “observations” were then sent to a number of “hounds” who applied various methodologies to try to recover a number of stellar properties, namely radius, mass, age, mean density, surface gravity, the radius of the base of the convection zone (BCZ), and the acoustic radii of the BCZ, the He II zone, and the  $\Gamma_1$  peak between the He I and He II zones. One of the original aspects to this exercise was that the hounds came in three groups: those who applied grid (or forward) modelling, those who applied glitch analysis, and those who applied inversions. The basic conclusions of the exercise was that grid modelling leads to more accurate but also more model-dependent results and that it is possible to meet PLATO 2.0 requirements for a star similar to the sun (Reese et al. 2016).

### A.3 CNAP duties (*i.e.* “tâche de service”)

Within the context of my current position as an associate astronomer, I carry out an astronomer’s duty, *i.e.* a “tâche de service” in French. My duty is to head workpackage

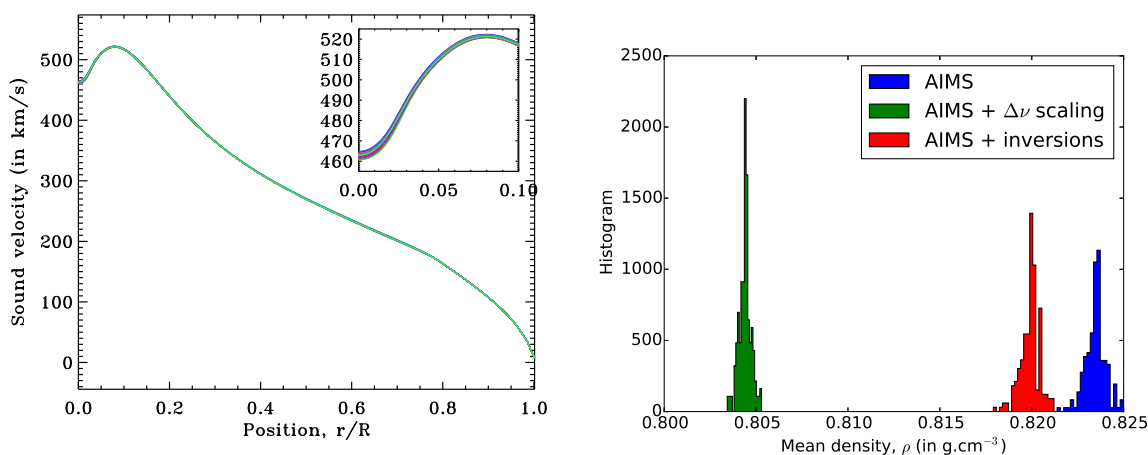


Figure A.3: Sound velocity profiles of interpolated models (left panel) and various mean densities (right panel), representative of KIC 10963065.

321000 for PLATO, *i.e.* “PSF<sup>5</sup> modelling”. The goal is to obtain detailed images of the PSFs across the entire field-of-view (FOV) for PLATO. Although these can be modelled on earth using the optical design of the PLATO telescopes, imperfections in the actual alignment of the optical components and any further deterioration as a result of launch vibrations and space conditions make it necessary to periodically recalibrate the PSFs while the PLATO mission is in space. These detailed PSFs will then intervene in the determination of optimal masks around observed stars, as well as various post-treatments of the data, such as reducing the effects of satellite jitter and correcting for long term drifts such as relativistic aberration.

The basic strategy for obtaining high-resolution reconstructions of the PSFs can be broken down into two parts:

- **PSF inversions:** the goal of this step is to go from low resolution images, obtained with the PLATO CCDs, to a high-resolution image of a PSF. Indeed, the various post-treatments based on the PSFs require a resolution at least 10 times greater than that of the CCDs. The currently adopted strategy consists in carrying out a microscanning session in which a series of *imagettes* (*i.e.* small images) is obtained with subpixel displacements (see left panel of Fig. A.4). These imagettes are then supplied to an inversion program which reconstructs the high resolution PSF. This procedure is carried out for a number of reference stars across the FOV.
- **PSF interpolation:** the goal of this step is to interpolate the PSF to stars at any position in the FOV using the inverted PSFs for the reference stars. We note that the FOV is relatively large – approximately 20° in radius for one PLATO telescope. Hence the PSF will vary substantially across the FOV. Besides interpolation in position, it may also be necessary to interpolate according to stellar temperature as this affects their colour and hence the PSFs.

Work for workpackage 321000 initially began with J. J. Green who first investigated various voxel (*i.e.* volume element) type inversions to combine images from multiple stars

<sup>5</sup>Point Spread Function.



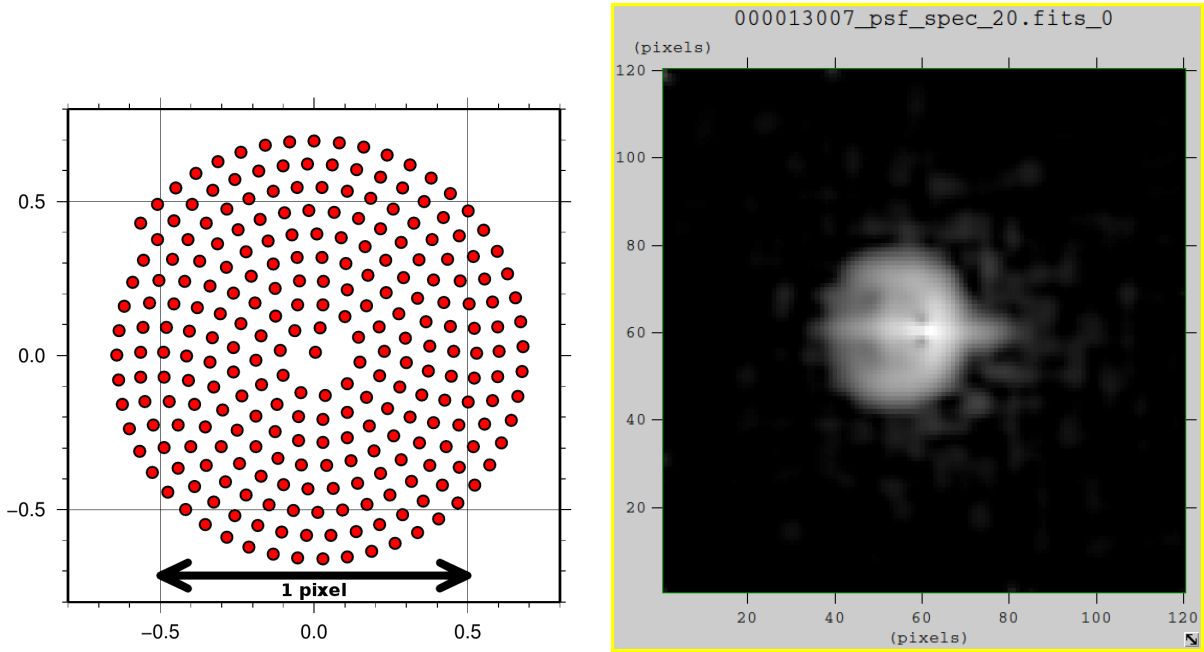


Figure A.4: (Left) Subpixel displacements for microscanning strategy (taken from Green, J. J. 2011a). (Right) Inverted PSF using the weighted positive RLS scheme (Reese, D. R. 2017c).

at the same distance from the centre of the FOV but in different directions (Green, J. J. 2010b,a). The underlying assumption is that the PSF would be the same for these targets apart from a rotation. However, a slight offset of the CCD from the focal plane and departures from planarity may invalidate this assumption. Hence, J. J. Green investigated the possibility of applying a microscanning strategy (Green, J. J. 2011a). J. Auriac and he put together various iterative procedures for inverting the series of imagettes from the microscanning session and obtain a detailed image of the PSF (Green, J. J. 2011b, Auriac, J. 2011). Later on, Ouazzani et al. (2015a) extended this study to different microscanning strategies and including a more realistic treatment of satellite jitter in the imagettes. I then became leader of the workpackage and looked into PSF interpolation across the FOV using the same strategy as in AIMS, *i.e.* using a Delaunay tessellation (Reese, D. R. 2016). Figure A.5 shows the interpolation errors across one of the quadrants of the PLATO FOV. I then went on to investigate regularised-least squares (RLS) inversions including a positivity constraint (the PSF cannot take on negative values) using a uniform Laplacian for the regularisation (Reese, D. R. 2017a) and a weighted Laplacian (Reese, D. R. 2017c). The latter approach yields on average better results than the iterative methods as it allows an explicit control over the regularisation rather than an implicit one. The right panel of Fig. A.4 shows an example of an inverted PSF. In (Reese, D. R. 2017b), I describe an alternate algorithm for carrying out the weighted positive RLS inversion which is substantially faster for our particular problem than what could be achieved with the ALGLIB library<sup>6</sup>. Currently, I'm working on a strategy for inverting PSFs when nearby stars contaminate the imagettes. This strategy incorporates a deconvolution in the inversion, but requires prior knowledge of the relative positions and luminosities of

<sup>6</sup><http://www.alglib.net/>

the contaminants.

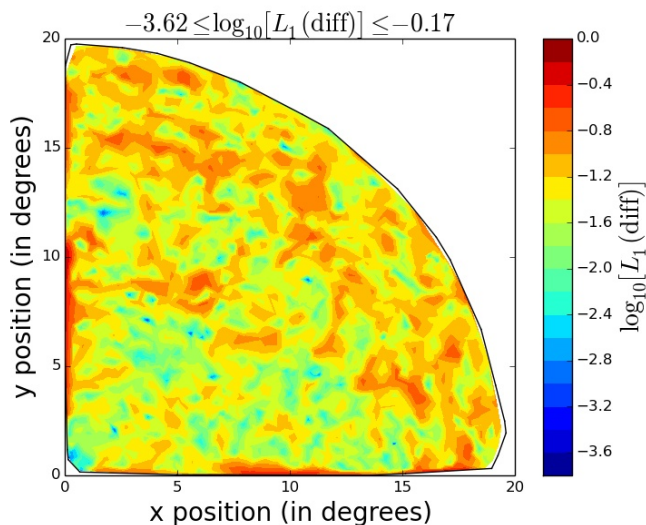


Figure A.5: PSF interpolation errors across one quadrant in PLATO's field-of-view.

## A.4 Teaching

A detailed list of the past and present teaching responsibilities is provided in my CV (see App. B). Hence, this section will briefly address some of the basic aspects of my approach to teaching. So far, most of my teaching has been tutorials in which I help students work through various maths or physics exercises. In sufficiently small classes, I will strive to obtain interaction with the students by either asking them questions as I explain how to solve the problem, or by asking volunteers to work through the problem on the blackboard. I also go around checking their progress and correcting them if need be. My goal is for students to work through the problems themselves and try to understand the principles behind, rather than relying on rote memorisation. On the few occasions where I have given lectures, I have tried to carefully think through the organisation of my lecture so that the students can have clear idea of the underlying train of thought.

## A.5 Supervision

### A.5.1 Supervision of Master's students

From 2012 to 2013, M.-A. Dupret and I supervised G. Buldgen's year 2 Master's project (or internship). The goal of his project was to extend the mean density inversions described in Reese et al. (2012) to two other quantities, namely the acoustic radius and an age indicator based on the small frequency separation. Accordingly, I taught him inversion theory by having him work through simplified examples, derive the variational principle, and obtain explicit expressions for some of the simpler structural kernels. A detailed proofreading of his work allowed me to correct mistakes or show simpler ways of doing certain mathematical manipulations. I also had him implement these inversions in the the `InversionKit` code, which meant he had to learn Java. Of course, I explained the

structure of the code to him and helped him with debugging the code when necessary. This work was subsequently pursued during his PhD and lead to the publication of an article (Buldgen et al. 2015b).

In 2016, I supervised B. Herbert’s year 1 Master’s project. The goal of his project was to set up an interface between AIMS and OSM<sup>7</sup>, a python code written by R. Samadi which uses a Levenberg-Marquardt algorithm to find optimal stellar models which fit a set classic and seismic constraints. Although the AIMS code obtains a global view of the stellar parameter space, it is subject to interpolation errors which stem from interpolating in a grid of models. In contrast, OSM uses stellar models from a stellar evolutionary code at each iteration, thereby avoiding interpolation. However, the Levenberg-Marquardt algorithm is local and can easily be trapped by local minimum. Hence by combining the two codes, one can get the best of both worlds, *i.e.* carrying a global exploration of parameter space, but obtaining optimised solutions which do not involve model interpolation. B. Herbert therefore made the necessary modifications to AIMS so that it would produce the necessary output files with which to start the OSM code. He then went on to investigate several stars using the two codes together, and also tested the effects of different surface correction recipes on derived stellar properties.

In addition to supervising the above two students, I helped G. Mirouh with his year 2 Master’s project which took place from 2012 to 2013. Indeed, he used the TOP code in its adiabatic version to fit the pulsation spectrum of Rasalhague ( $\alpha$  Ophiuchi). I helped him learn how to use the code, produced a brief documentation to go with it, supplied him with a program to calculate mode visibilities based on Reese et al. (2013), and helped him with debugging when necessary. He produced a first set of results<sup>8</sup> including mode frequencies, visibilities, and damping rates based on the quasi-adiabatic approximation, which he then compared with Rasalhague’s pulsation spectrum (Mirouh et al. 2014).

Finally, I soon will be supervising P. Houdayer’s year 1 Master’s project. He will work on extending a program I wrote which is able to calculate the centrifugal deformation of a rotating star or planet, starting from a 1D non-rotating model. The method applied in the program is very close to the SCF method (*e.g.* Jackson et al. 2005, MacGregor et al. 2007) in which Poisson’s equation is solved alternatively with finding the level surfaces, *i.e.* the isopotentials, and iterating till convergence. He will extend the code so that it can handle discontinuous models, thus making it applicable to planets such a Jupiter which may have a solid core. This can subsequently be included in programs such as CEPAM (Guillot & Morel 1995) which calculates the evolution of planets. Another use of the code is to generate deformed models of evolved stars for asteroseismology, while waiting for ESTER to fully include the effects of stellar evolution.

## A.5.2 Supervision of PhD students

From 2014 to 2017, G. Buldgen carried out his PhD. M.-A. Dupret was his supervisor and I his co-supervisor. During this time period, G. Buldgen extended his work on inversions to new integrated quantities (Buldgen et al. 2015a, 2018) thus requiring the derivation of new structural kernels (Buldgen et al. 2017b). He applied these inversions to the 16 Cyg

<sup>7</sup>“Optimal Stellar Models” – see <https://pypi.python.org/pypi/osm/>

<sup>8</sup>Later on, G. Mirouh would pick up on this work again, but using the non-adiabatic version of TOP, as described in Sect. 3.6.

binary system (Buldgen et al. 2016a,b), the targets from the SPACEINN hare-and-hounds exercise (Reese et al. 2016), and Legacy targets (Buldgen et al. 2017a), thus showing how they could further constrain stellar properties such as mass, radius, and age. He also carried out detailed profile inversions of an entropy proxy in the sun (Buldgen et al. 2017e) and the Ledoux discriminant to further constrain the solar tachocline (Buldgen et al. 2017c). His inversions on the solar metallicity (Buldgen et al. 2017d) favour the newer, lower abundances, although the uncertainties remain large. Given that I had moved away from Liège, I kept track of his work through email correspondence and various trips. A careful proofreading of his articles allowed me to improve their clarity and sometimes suggest new ideas. Thanks to his perseverance, hard work, and aptitude for theoretical work, he achieved brilliant results and has been able to impose himself as a reference in the domain of asteroseismic inversions.

Currently, I'm co-supervising K. Bouchaud's PhD. He started his PhD in 2017 in Nice under the supervision of A. Domiciano de Souza, working on spectroscopy and interferometry of rapidly rotating stars. This summer he will move over to Meudon to carry out the second part of his PhD, namely using asteroseismology to constrain such stars. Given how difficult this problem is, it will be necessary to use mode identification techniques and to carefully choose which stellar targets to study. Accordingly, he will also work on improving the theoretical predictions for line profile variations by including stellar atmospheres rather than using the simplified treatment described in Sect. 3.5.2.

I've also assisted PhD students with some of their work. For instance, I supplied the TOP pulsation code to K. Burke so that she could compare full 2D pulsation calculations with a perturbative approach in realistic models from the ASTEC<sup>9</sup> code (Burke et al. 2011). I also helped R.-M. Ouazzani by supplying her with models of rapidly rotating polytropes, interpolated to a dense radial suitable for finite-differences so that she could apply the ACOR<sup>10</sup> pulsation code to these models. She then compared her pulsation modes and frequencies with the results from TOP, thus validating her code (Ouazzani et al. 2012).

---

<sup>9</sup>Aarhus STellar Evolution code (Christensen-Dalsgaard 2008).

<sup>10</sup>Adiabatic Code of Oscillation including Rotation.



# Appendix B

## Curriculum Vitae

Daniel Roy REESE  
LESIA  
Observatoire de Paris, Section de Meudon  
5, place Jules Janssen  
92195 MEUDON Cedex, FRANCE

Associate astronomer  
**Tel:** +33 (0)1 45 07 78 12  
**Email:** [daniel.reese@obspm.fr](mailto:daniel.reese@obspm.fr)

### Personal information

- Born on January 4, 1980, at Neuilly-sur-Seine
- Nationalities: French and American
- Single
- Bilingual: French, English

### Research activities

2015- Associate astronomer  
2014-2015 Postdoc at the University of Birmingham, supported by the SpaceInn network  
2011-2013 Postdoc at the Université de Liège  
2009-2011 Postdoc at the Observatoire de Paris, at Meudon, supported by the CNES  
2006-2009 Postdoc at the University of Sheffield, supported by the HELAS network and the UK Science and Technology Facilities Council

### University studies

2003-2006 Astrophysics PhD, at the Université Toulouse III, Paul Sabatier  
Title: “La modélisation des oscillations d’étoiles en rotation rapide”  
Directed by: M. Rieutord (supervisor) and F. Lignières (cosupervisor)  
2002-2003 DEA (= 2<sup>nd</sup> year Master) in Astrophysics, Planétology, and Space sciences and technology, Toulouse  
2000-2003 Engineering school: Supaéro (ENSAE), Toulouse  
1998-2000 Preparatory classes (MPSI and MP) at the Lycée Pierre de Fermat, Toulouse

**Prize**

2007 Pierre Maury Prize for the PhD thesis from the “Académie des Sciences, Inscriptions et Belles-Lettres de Toulouse”

**Supervision**

2017- PhD cosupervision of K. Bouchaud  
 2013-2017 PhD cosupervision of G. Buldgen  
 2017 Internship supervision of P. Houdayer (3<sup>rd</sup> year university student)  
 2016 Internship supervision of B. Herbert (1<sup>st</sup> year Master’s student)  
 2012-2013 Internship supervision of G. Buldgen (2<sup>nd</sup> year Master’s student)

**Teaching activities**

2015-2017 courses, tutorials and hands-on sessions on inversions (1<sup>st</sup> year Master’s and PhD students) (51h)  
 2016-2017 c++ hands-on sessions for 2<sup>nd</sup> year Master’s students (44h)  
 2015-2017 remote training (“Fenêtres sur l’Univers”) (DU) (49h)  
 2016 oral physics tests for 1<sup>st</sup> year university students at the UPMC, Paris  
 2014-2015 supervision of c++ hands-on sessions and 3<sup>rd</sup> year student group project at the University of Birmingham (~ 60 h)  
 2007-2009 12 applied maths tutorials for 1<sup>st</sup> and 2<sup>nd</sup> year students at the University of Sheffield (each takes 1 h/week and lasts 1 semester)  
 2005 Math tutorial (12.5 h) for 1<sup>st</sup> year students at the Université Toulouse III, Paul Sabatier  
 2004-2006 Computer hands-on sessions (15 h) for statistical physics at Supaéro

**Teaching at young scientists’ schools**

**Reese, D. R.**, Lebreton, Y. 2018. “Stellar age determination hands-on-session”. 5<sup>th</sup> International Young Astronomers School: Scientific Exploitation of the Gaia Data. Paris.  
**Reese, D. R.**. 2016. “Stellar Inversion Techniques”. Asteroseismology and Exoplanets: Listening to the Stars and Searching for New Worlds. Horta, Faial, Açores. arXiv:1711.01798.  
 Lund, M. N., **Reese, D. R.**. 2016. “AIMS: Asteroseismic Inference on a Massive Scale – A tutorial”. Asteroseismology and Exoplanets: Listening to the Stars and Searching for New Worlds. Horta, Faial, Açores. arXiv:1711.01896.

**Responsibilities**

## • PLATO

- WP 374220 then WP 124200 (2010 onwards): developement and implementation of seismic inversion methods
- WP 321000 (2015 onwards): PSF modelling (see Sect. A.3)

- **SpaceInn** (2014-2015)
  - organisation of a hare-and-hounds exercise in order to evaluate various methods for estimating stellar parameters from classical and seismic data
  - development of scientific software (see Sect. A.2)
- **HELAS** (2006-2009)
  - participation in the “Low degree and low frequency modes” (La Palma, 2007) and “The Acoustic Solar Cycle” (Birmingham, 2009) workshops
  - creation of a website for the global helioseismology branch in HELAS
  - development of scientific software (see Sect. A.1)

### Rank A publications

**Number:** 40 (for which 11 are first-author publications)

- Nsamba, B., Campante, T. L., Monteiro, M. J. P. F. G. et al. “Asteroseismic modelling of solar-type stars: internal systematics from input physics and surface correction methods”, MNRAS, in press (6<sup>th</sup> author).
- Guillot, T., Miguel, Y.; Militzer, B. et al. 2018. “A suppression of differential rotation in Jupiter’s deep interior”, Nature 555, Issue 7695, 227-230 (14<sup>th</sup> author).
- Buldgen, G., **Reese, D. R.**, Dupret, M. A. 2018. “Constraining convective regions with asteroseismic linear structural inversions”, A&A 609, A95, 13 pages.
- Buldgen, G., Salmon, S. J. A. J., Noels, A. et al. 2017 “Seismic inversion of the solar entropy: A case for improving the Standard Solar Model”, A&A 607, A58, 5 pages (5<sup>th</sup> author).
- Buldgen, G., Salmon, S. J. A. J., Godart, M. et al. 2017, “Inversions of the Ledoux discriminant: a closer look at the tachocline”, MNRAS 472, L70-L74 (7<sup>th</sup> author).
- Buldgen, G., Salmon, S. J. A. J., Noels, A. et al. 2017. “Determining the metallicity of the solar envelope using seismic inversion techniques”, MNRAS 472, 751-764 (6<sup>th</sup> author).
- García Hernández, A., Suárez, J. C., Moya, A. et al. J. 2017. “Precise surface gravities of  $\delta$  Scuti stars from asteroseismology”, MNRAS 471, L140-L144 (6<sup>th</sup> author).
- Wahl, S. M., Hubbard, W. B., Militzer, B. et al. 2017. “Comparing Jupiter interior structure models to Juno gravity measurements and the role of a dilute core”, GRL 44, issue 10, page 4649-4659 (9<sup>th</sup> author).
- Reese, D. R.**, Lignières, F., Ballot, J. et al. 2017. “Frequency regularities of acoustic modes and multi-colour mode identification in rapidly rotating stars”, A&A 601, A130, 14 pages.
- Silva Aguirre, V., Lund, M. N., Antia, H. M. et al. 2017. “Standing on the Shoulders of Dwarfs: the Kepler Asteroseismic LEGACY Sample. II. Radii, Masses, and Ages” ApJ 835, 173, 18 pages (8<sup>th</sup> author).
- Buldgen, G., **Reese, D. R.**, Dupret, M. A. 2017. “Analysis of the linear approximation of seismic inversions for various structural pairs”, A&A 598, A21, 14 pages.



- Buldgen, G., Salmon, S. J. A. J., **Reese, D. R.**, Dupret, M. A. 2016. “In-depth study of 16CygB using inversion techniques”, A&A 596, A73, 14 pages.
- Reese, D. R.**, Chaplin, W. J., Davies, G. R. et al. 2016. “SpaceInn hare-and-hounds exercise: Estimation of stellar properties using space-based asteroseismic data”, A&A 592, A14, 27 pages.
- Buldgen, G., **Reese, D. R.**, Dupret, M. A. 2015. “Constraints on the structure of 16 Cygni A and 16 Cygni B using inversion techniques”, A&A 585, A109, 12 pages.
- Buldgen, G., **Reese, D. R.**, Dupret, M. A. 2015. “Using seismic inversions to obtain an indicator of internal mixing processes in main-sequence solar-like stars”, A&A 583, A62, 14 pages.
- García Hernández, A., Martín-Ruiz, S., Monteiro, M. J. P. F. G. et al. 2015. “Observational  $\Delta\nu - \rho$  Relation for  $\delta$  Sct Stars using Eclipsing Binaries and Space Photometry”, ApJL 811, L22, 6 pages (5<sup>th</sup> author).
- Coelho, H. R., Chaplin, W. J., Basu, S. et al. 2015. “A test of the asteroseismic  $\nu_{\max}$  scaling relation for solar-like oscillations in main-sequence and sub-giant stars”, MNRAS 451, p. 3011-3020 (6<sup>th</sup> author).
- Reese, D. R.** 2015. “Inequalities on stellar rotational splittings derived from assumptions on the rotation profile”, A&A 578, A37, 15 pages.
- Buldgen, G., **Reese, D. R.**, Dupret, M.-A., Samadi, R. 2015. “Stellar acoustic radii, mean densities and ages from seismic inversion techniques”, A&A 574, A42, 16 pages.
- Salmon, S. J. A. J., Montalbán, J., **Reese, D. R.** et al. 2014. “The puzzling new class of variable stars in NGC 3766: old friend pulsators?”, A&A 569, A18, 8 pages.
- Deheuvels, S., Doğan, G., Goupil, M. J. et al. 2014. “Seismic constraints on the radial dependence of the internal rotation profiles of six Kepler subgiants and young red giants”, A&A 564, A27, 24 pages (16<sup>th</sup> author).
- García, R. A., Pérez Hernández, F., Benomar, O. et al. 2014. “Study of KIC 8561221 observed by Kepler: an early red giant showing depressed dipolar modes”, A&A 563, A84, 17 pages (20<sup>th</sup> author).
- Reese, D. R.** 2013. “Stable higher order finite-difference schemes for stellar pulsation calculations”, A&A 555, A148, 12 pages.
- Reese, D. R.**, Prat, V., Barban, C. et al. 2013. “Mode visibilities in rapidly rotating stars”, A&A 550, A77, 28 pages.
- Ouazzani, R.-M., Dupret, M.-A., **Reese, D. R.**, 2012. “Pulsations of rapidly rotating stars. I. The ACOR numerical code”, A&A 547, A75, 14 pages.
- Briquet, M., Neiner, C., Aerts, C. et al. 2012. “Multisite spectroscopic seismic study of the  $\beta$  Cep star V2052 Ophiuchi: inhibition of mixing by its magnetic field”, MNRAS 427, p. 483-493 (6<sup>th</sup> author).
- Pasek, M., Lignières, F., Georgeot, B., **Reese, D. R.**, 2012. “Regular Oscillation Sub-spectrum of Rapidly Rotating Stars”, A&A 546, A11, 13 pages.
- Deheuvels, S., García, R. A., Chaplin, W. J., et al. 2012. “Seismic Evidence for a Rapidly Rotating Core in a Lower-giant-branch Star Observed with Kepler”, ApJ 756, 19, 16 pages (12<sup>th</sup> author).

- Reese, D. R.**, Marques, J. P., Goupil, M. J. et al. 2012. “Estimating stellar mean density through seismic inversions”, *A&A* 539, A63, 18 pages.
- Pasek, M., Georgeot, B., Lignières, F., **Reese, D. R.**. 2011. “Regular Modes in Rotating Stars”, *Ph. Rev. L.* 107, 12, 121101, 5 pages.
- Burke, K. D., **Reese, D. R.**, Thompson, M. J. 2011. “On the effects of rotation on acoustic stellar pulsations: validity domains of perturbative methods and close frequency pairs”, *MNRAS* 414, p. 1119-1126.
- Suárez, J. C., Goupil, M. J., **Reese, D. R.**, et al. 2010. “On the Interpretation of Echelle Diagrams for Solar-like Oscillations Effect of Centrifugal Distortion”, *ApJ* 721, p. 537-546.
- Ballot, J., Lignières, F., **Reese, D. R.**, Rieutord, M. 2010. “Gravity modes in rapidly rotating stars. Limits of perturbative methods”, *A&A* 518, A30, 8 pages.
- Reese, D. R.**, Thompson, M. J., MacGregor, K. B. et al. 2009. “Mode identification in rapidly rotating stars”, *A&A* 506, p. 183-188.
- Reese, D. R.**, MacGregor, K. B., Jackson, S. et al. 2009. “Pulsation modes in rapidly rotating stellar models based on the Self-Consistent Field method”, *A&A* 506, p. 189-201.
- Charpinet, S., Van Grootel, V., **Reese, D.**, et al. 2008. “Testing the forward modeling approach in asteroseismology. II. Structure and internal dynamics of the hot B subdwarf component in the close eclipsing binary system PG 1336-018”, *A&A* 489, p. 377-394.
- Reese, D.**, Lignières, F., Rieutord, M. 2008. “Regular patterns in the acoustic spectrum of rapidly rotating stars” , *A&A* 481, p. 449-452.
- Reese, D.**, Lignières, F., Rieutord, M. 2006. “Acoustic oscillations of rapidly rotating polytropic stars. II. Effects of the Coriolis and centrifugal accelerations” , *A&A* 455, p. 621-637 + a 5 page appendix.
- Lignières, F., Rieutord, M., **Reese, D.** 2006. “Acoustic oscillations in rapidly rotating polytropic stars. I. Effects of the centrifugal distortion.” , *A&A* 455, 607-620 + a 3 page appendix.
- Reese, D.**, Rincon, F., Rieutord, M. 2004. “Oscillations of magnetic stars. II. Axisymmetric toroidal and non-axisymmetric shear Alfvén modes in a spherical shell” . *A&A* 427, 279-292 + a 2 page appendix.

## Conferences

### With proceedings

- 6 invited contributions
- 11 other first-author contributions
- 26 contributions as co-author

### Without proceedings

- 2 invited contributions
- 6 other first-author contributions
- 5 contributions as co-author